Biomechanics of the Human Chorioamnion

by

Thibault Philippe Prévost

Ingénieur de l'Ecole Polytechnique
Ecole Polytechnique (2004)

Submitted to the Department of Materials Science and Engineering
in partial fulfillment of the requirements for the degree of

Master of Science

at the

MASSACHUSETTS INSTITUTE OF TECHNOLOGY

February 2006

Signature of Author .....
Department of Materials Science and Engineering
January 31, 2006

Certified by .....
Subra Suresh
Ford Professor of Engineering
Thesis Supervisor

Certified by .....
Simona Socrate
Assistant Professor of Mechanical Engineering
Thesis Supervisor

Accepted by .....
Samuel M. Allen
POSCO Professor of Physical Metallurgy
Chair, Departmental Committee on Graduate Students

Biomechanics of the Human Chorioamnion

by

Thibault Philippe Prévost

Submitted to the Department of Materials Science and Engineering
on January 31, 2006, in partial fulfillment of the
requirements for the degree of
Master of Science

Abstract

The human fetal membrane, namely the chorioamnion, is the structural soft tissue retaining the amniotic fluid and the fetus during pregnancy. Its biomechanical integrity is crucial for maintaining a healthy gestation and a successful delivery. The premature rupture of the fetal membrane (PROM) can result in serious perinatal complications. Despite extensive research in this field, the mechanical and biochemical processes governing the membrane deformation and failure remain poorly understood. The aim of this study is to characterize the mechanical behavior of the chorioamnionic tissue along with its biochemical properties, through mechanical testing and biochemical analyses. In order to accomplish this goal, specific mechanical and biochemical testing protocols were developed. *In vitro* mechanical testing was performed on samples from seven patients under different uniaxial and biaxial loading conditions. Significant relaxation was noted under uniaxial loading while very limited creep was observed under biaxial loading. Biochemical measurements such as collagen and sulfated glycosaminoglycan contents were also obtained. In addition, a microstructurally based constitutive model for the fetal membrane is proposed. The model allows for nonlinear hyperelastic response at large deformation. We also propose a framework to capture the time-dependent response of the tissue. The model was implemented in a finite element formulation to allow three-dimensional simulations of membrane deformation.

Thesis Supervisor: Subra Suresh
Title: Ford Professor of Engineering

Thesis Supervisor: Simona Socrate
Title: Assistant Professor of Mechanical Engineering

Contents

List of Figures

List of Tables

Acknowledgments

I first thank Professor Subra Suresh, whose counsel and support made this project possible. I am also truly indebted to Professor Simona Socrate for her extraordinary guidance, and her constant, enthusiastic support. Her invaluable help in the modeling has been critical to the success of this project. I am as much indebted to Dr. Michael House without whom none of the in vitro experiments could have been carried out.

My deepest gratitude goes to Kristin Myers for kindly allowing me to use her laboratory facilities and for so patiently and skillfully guiding me in the mechanical and biochemical testing. I am also truly grateful to Peter Morley from the MIT Machine Shop whose help in the design of the mechanical apparatus was essential.

Let me also warmly thank Dr. Hidemi Kato for his crucial contribution in performing mechanical tests. His patience and support during uncountable hours of testing, along with his critical reviewing, have greatly contributed to the success of this project.

I would neither forget to thank Professor Michelle Oyen, Dr. Steven Calvin, Orian Regnier and Olivier Vernhet, for their crucial assistance in the successful starting of the mechanical testing. Special thanks to Dr. Steven Calvin for his scanning electron microscopy pictures of the chorioamnion.

I am also truly grateful for the fruitful contributions of Martin Skelton to the MATLAB image analysis.

Finally, I would like to thank all my friends who have made the past twelve months at MIT a wonderful time.

Chapter 1

Motivation and Background

1.1 Introduction

Preterm delivery occurs in about 11% of all pregnancies in the United States and is one of the leading causes of perinatal morbidity and mortality [1]. Despite extensive research in this field, the preterm birth rate has continued to rise steadily, increasing by more than 15% over the past two decades [2]. Among the critical factors accounting for preterm delivery, are preterm labor (i.e. premature onset of regular uterine contractions with progressive cervical dilatation), rupture of the fetal membranes, cervical malfunction, bleeding, infection, fetal anomaly or *abruptio placentae*. Premature rupture of the membranes (PROM) alone is associated with 30 to 40 percent of all preterm births and is considered one of the main obstetrical complications resulting in preterm delivery [3]. Its clinical prevention, assessment and treatment remain major challenges in modern obstetrics.

1.2 Anatomy and structure

The fetal membrane, also referred to as the chorioamnionic (CA) membrane, is the structural soft tissue retaining the fetus within the uterine cavity during pregnancy (Figure 1-1). The membrane itself consists of two main layers, the amnion (inner layer) retaining the amniotic fluid, and the chorion (outer layer) facing the uterine decidua (Figure 1-1). Its biomechanical

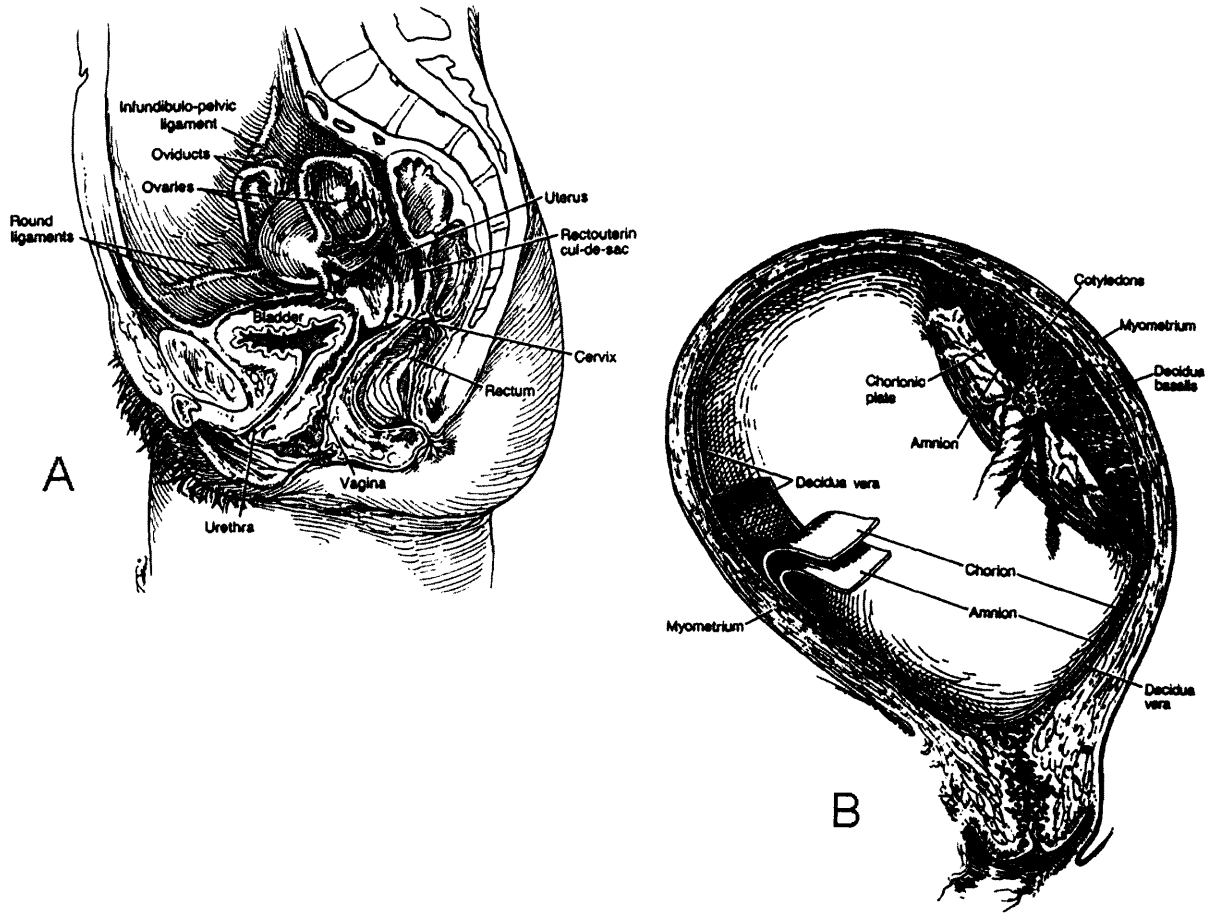

Figure 1-1: (A) Sagittal section of the pelvis of an adult woman. (B) Uterus of pregnant woman showing normal placenta in situ. Modified from "Williams Obstetrics" [4].

integrity is crucial for maintaining a healthy gestation: not only acting as a protective "mechanical envelope" preventing the amniotic fluid and the conceptus from leaving the cavity, it also allows for solute and fluid exchange from maternal blood to the fetus through its numerous microscopic vascular projections or microvilli.

Its maturation throughout gestation corresponds to a complex, yet poorly understood, process combining tissue growth, biochemical changes, and structural remodeling. Until near the end of the third month of gestation, the chorion laeve remains a distinct entity, separated from the amnion by the exocoelomic cavity and from the decidua vera by the uterine cavity (Figure 1-2). By the fourth month, the enlarging sac fills the entire uterine cavity and, with fusion of the decidua vera and capsularis, the cavity is obliterated. The amnion and chorion also come in close contact, forming a single bilayer (the chorioamnion) that continues to develop as a whole with the growing fetus until term.

The normal organization and microscopic anatomy of the CA membrane (Figure 1-3) have been described in detail by Bourne et al [5–8]. The amnion, which is normally 20 to 80 μm in thickness, accounts for the essential part of the CA membrane's strength [9]. It is composed of five sublayers: the epithelium, the basement membrane, the compact layer, the fibroblast layer and the spongy layer. The epithelium is the innermost layer in contact with the amniotic fluid. It consists of a single layer of cells adherent to the basement membrane. Beneath the epithelium lie the compact and fibroblast layers constituting 60 to 80 % of the amnion's thickness. They essentially consist of a dense network of collagen fibrils responsible for the tissue resilience. The intermediate layer lying at the interface of the amnion and the chorion is referred to as the spongy layer, rich in hydrated proteoglycans.

The chorion, which is 100 to 500 μm thick, is a soft cellular structure resembling a typical epithelial membrane and consisting of three main layers[1]. Adherent to the trophoblast layer (in contact with the maternal decidua), the basement membrane provides support for the reticular layer which forms the majority of the chorion thickness (Figure 1-3).

[1]The additional "cellular layer" labelled as such by Bourne can be considered as part of the reticular layer [3,10].

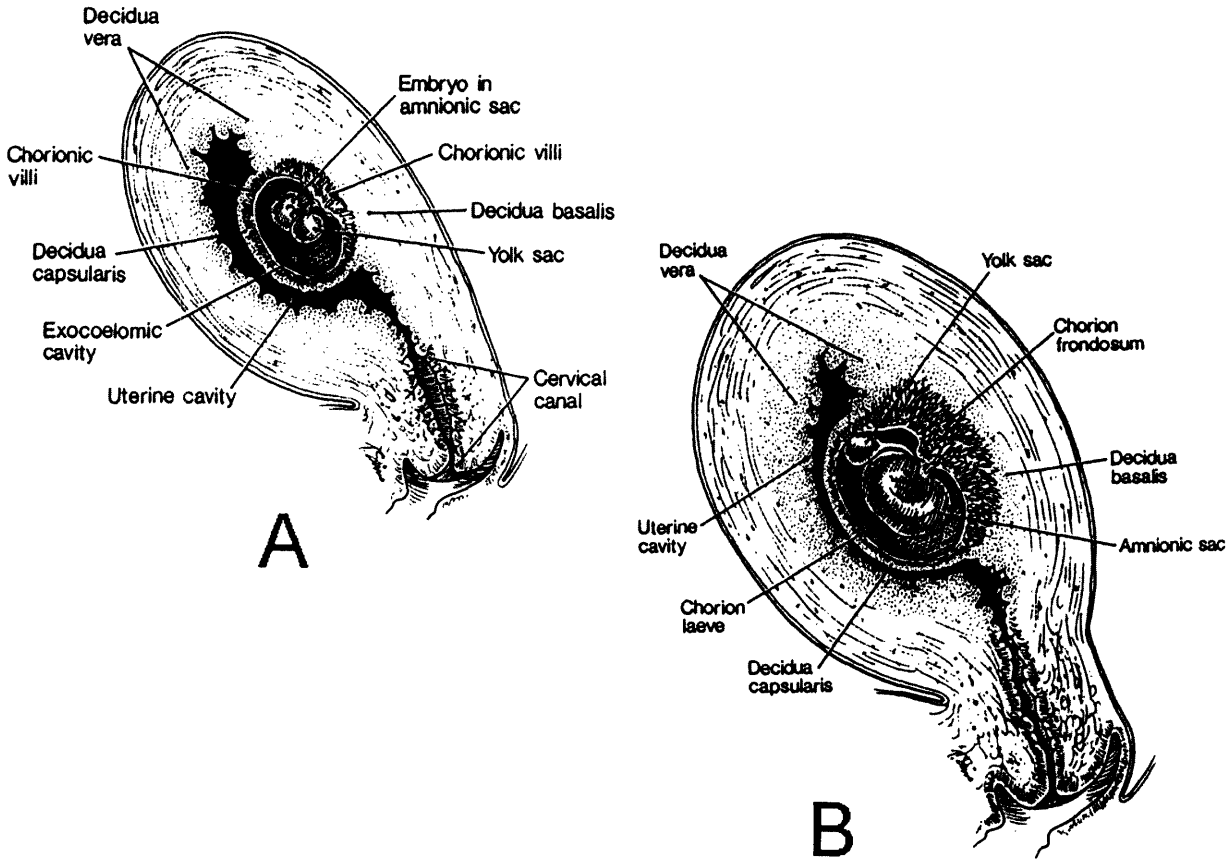

Figure 1-2: Illustration showing chorionamnionic sac in uterus at early (Figure A) and more advance (Figure B) stages of pregnancy. Modified from "Williams Obstetrics" [4].

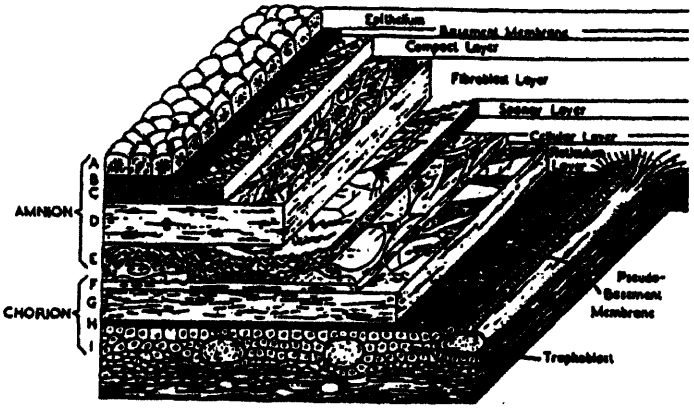

Figure 1-3: Schematic section through human chorioamnion. A: Epithelium. B: Basement membrane. C: Compact layer. D: Fibroblast layer. E: Spongy layer. F: Cellular layer. G: Reticulum layer. H: Pseudo-basement membrane. I: Trophoblast layer. From Bourne GL [7].

1.3 Extracellular matrix components of the fetal membranes

The extracellular matrix (ECM) is the organized assembly of macromolecules surrounding the cells. Collagen and proteoglycan molecules are, along with elastin, fibronectin and laminin, the major components of the CA membrane ECM (Figure 1-4), accounting for the tissue integrity and macroscopic mechanical properties [11].

1.3.1 Collagens

Collagens are glycoproteins consisting of polypeptide chains, called α chains, characterized by the repeated Gly(Glycine)-X-Y amino-acid sequence (X and Y often referring to proline and hydroxyproline), that can assemble into stable triple helical structures (Figure 1-5). Their extensive post-translational modifications [12] lead to the formation of higher-order aggregates stabilized by covalent intra- and intermolecular crosslinks (Figure 1-6) via reactive hydroxylysine residues. These complex crosslinked macrofibers are the major contributors to the fetal membrane mechanical strength and resilience.

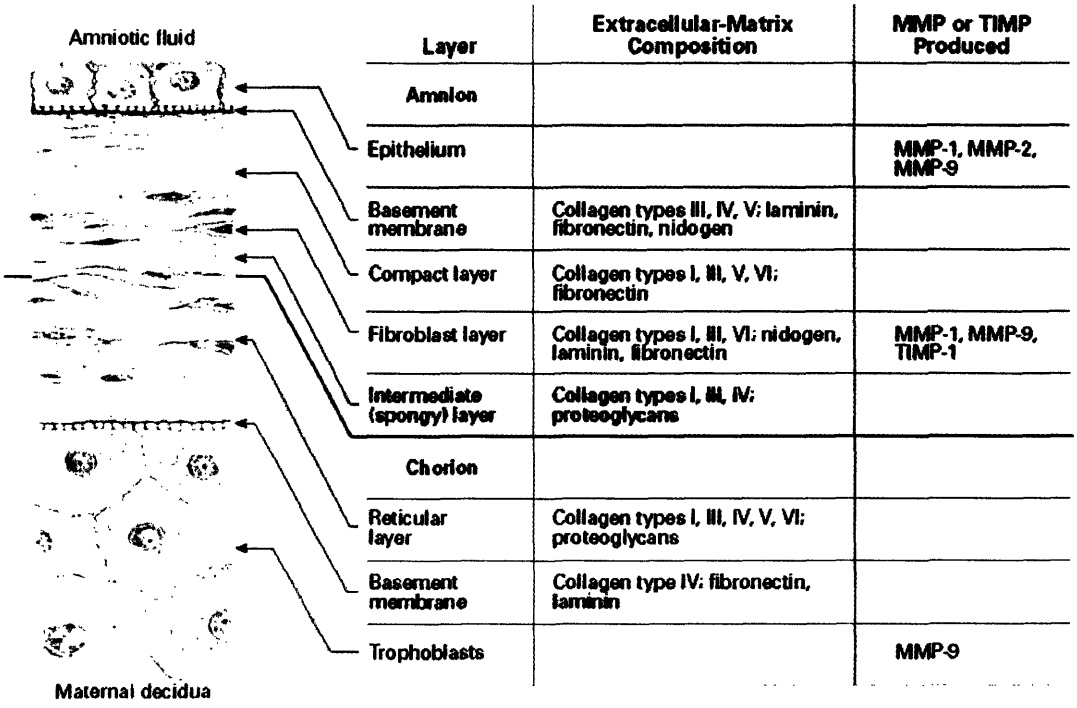

Layer	Extracellular-Matrix Composition	MMP or TIMP Produced
Amnion		
Epithelium		MMP-1, MMP-2, MMP-9
Basement membrane	Collagen types III, IV, V; laminin, fibronectin, nidogen	
Compact layer	Collagen types I, III, V, VI; fibronectin	
Fibroblast layer	Collagen types I, III, VI; nidogen, laminin, fibronectin	MMP-1, MMP-9, TIMP-1
Intermediate (spongy) layer	Collagen types I, III, IV; proteoglycans	
Chorion		
Reticular layer	Collagen types I, III, IV, V, VI; proteoglycans	
Basement membrane	Collagen type IV; fibronectin, laminin	
Trophoblasts		MMP-9

Figure 1-4: Schematic illustration of the CA membrane microstructure at term. The main ECM components of each layer, the production sites of matrix metalloproteinases (MMP), and tissue inhibitors of metalloproteinases (TIMP) are shown. From [3].

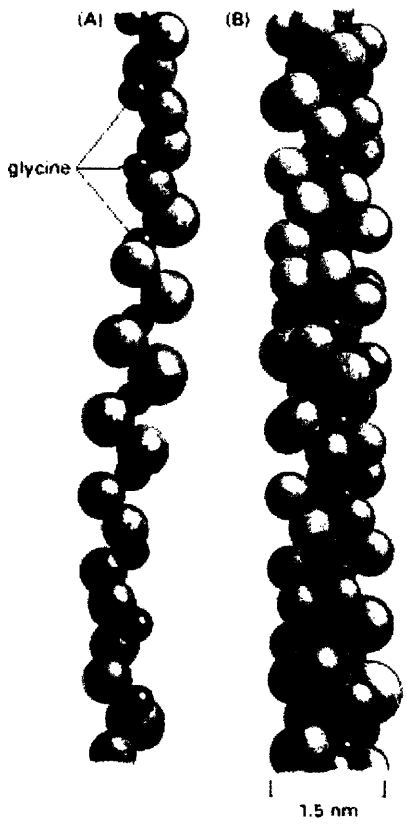

Figure 1-5: The structure of a typical collagen molecule. (A) Schematic section of a single collagen α chain in its left-handed helical conformation. The chain is about 1000 amino acids long. (B) Schematic section of a collagen molecule in which three α chains are wrapped around one another to form a triple-stranded helical rod. Glycine is the only amino acid small enough to occupy the crowded interior of the triple helix. Only a short length of the molecule is shown; the entire molecule is 300 nm long. From "Molecular Biology of the Cell" [12], chapter 19.

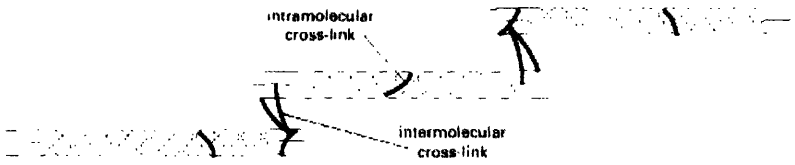

Figure 1-6: Cross-links formed between modified lysine side chains within a collagen fibril. From "Molecular Biology of the Cell" [12], chapter 19.

At least twenty genetically distinct types of collagen have been identified so far. Collagen types differ not only in their amino acid sequences but also in their spatial conformations conferring to them specific functional properties [12]. Collagen types I and III, together with smaller amounts of types IV, V and VI, are thought to be the main collagen components of the CA membrane (Figure 1-4). Collagens I, III and V belong to the same family, for which collagen molecules aggregate in quarter stagger arrangement to form higher order structures or fibers. They are presumed to be the primary components of the collagen network-like structure dominating the mechanical response of the tissue (Figure 1-7). Type IV collagen molecules form structural sheets within the basal lamina of the amniotic epithelium and the basement membranes of both amion and chorion. Finally, type VI collagen, whose functional properties remain uncertain, is thought to provide anchoring filaments at the interface of the amnion and chorion layers.

1.3.2 Proteoglycans

Proteoglycans are special glycoproteins (Figure 1-8) composed of a core protein to which sulfated polysaccharides or glycosaminoglycans (i.e. repeating disaccharide units) are covalently attached. Proteoglycans interact with collagen molecules to promote network crosslinking and to regulate collagen fibril formation.

Sulfated glycosaminoglycans such as dermatan and chondroitin sulfate, small proteoglycans like decorin or biglycan, and to a smaller extent, large proteoglycans such as versican and perlecan, have been identified in the CA membrane ECM [13,14]. A non-sulfated glycosaminoglycan, hyaluronic acid (hyaluronan, HA), is also present in the tissue. HA forms

Figure 1-7: Scanning electron micrograph of the amnionic layer showing the dense collagen fibril network of the compact layer beneath an epithelial cell layer. Micrograph picture taken by Dr. Steven Calvin at University of Minnesota.

complex networks and does not attach to a core protein. Essential contributors to the viscoelastic response of the connective tissues [15], proteoglycans are also said to play a structural role in maintaining the tissue integrity [16].

Decorin can be found in the amnion and also in the reticular layer of the chorion [14]. It binds to collagen types I and III, thereby enabling lateral organization of the collagen fibrils [18]. Biglycan, another small proteoglycan, mainly located in the trophoblastic part of the chorion, is thought to interact with type VI collagen [17]. Finally, the spongy layer at the interface between the amnion and the chorion is dominated by hyaluronan [14] which permits the amnion to slide on the underlying chorion, thereby alleviating shear stress along the interface [3].

1.3.3 Other glycoproteins and elastin

Fibronectin, laminin, and elastin are other important CA membrane ECM components [10]. However, their localization and function(s) are still subject to controversy.

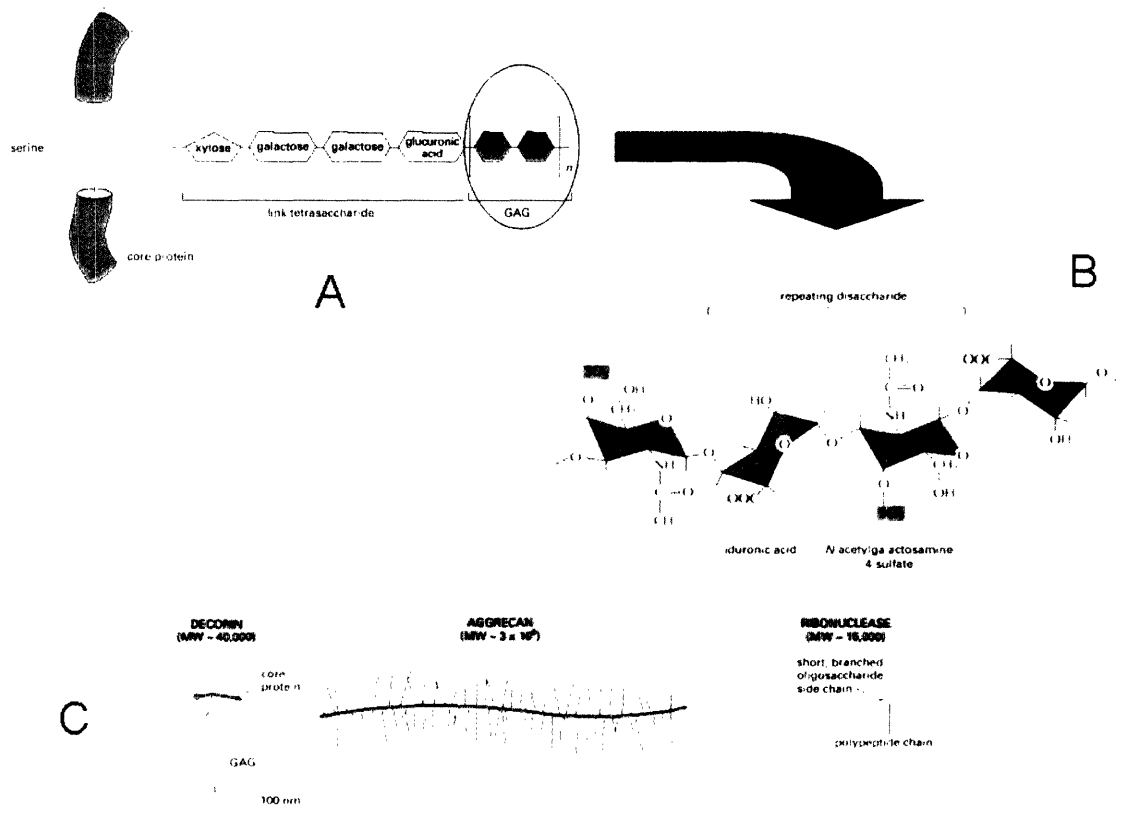

Figure 1-8: The linkage between a GAG chain and its core protein in a proteoglycan molecule (A); the repeating disaccharide sequence of a dermatan sulfate glycosaminoglycan chain (B); and examples of a small (decorin) and a large (aggrecan) proteoglycan found in the extracellular matrix, compared with a typical secreted glycoprotein molecule, pancreatic ribonuclease B (all three are drawn to scale). From "Molecular Biology of the Cell" [12], chapter 19.

Some of the fibronectin molecules present in the trophoblast layer of the chorion are believed to bind to ECM cells via specific integrin receptors [19], contributing to the chorion-decidua adhesion. Disruption of such fibronectin binding, occurring before or at term, may result in the separation of the chorion from the decidua in the lower uterine segment [20,21].

Laminins, an important component of basement membranes, also interact with ECM cells through integrin receptors [22,23]. Ensuring the "anchoring" of the epthelial cells to the underlying stroma via the basement membrane, they are thought to perform a significant strengthening function in the amnion [24].

Finally, elastin molecules, which correspond to complex insoluble proteins cross-linked to fibrillin-based microfibrils, are suspected to be abundant in the reticular and compact layers [25]. Having mechanical properties analogous to those of pure rubber, they may confer to the fetal membrane part of its intrinsic elasticity [10].

1.4 Premature Rupture Of Membranes (PROM)

1.4.1 Clinical definition and diagnosis

PROM is defined as the rupture of membranes before the onset of labor. Rupture occurring before 37 weeks of gestation is referred to as preterm PROM. Premature membrane rupture is confirmed clinically by the leakage of amniotic fluid in the posterior vaginal fornix or clear fluid passing from the cervical canal [1]. Its diagnosis can be performed mainly through:

- sterile speculum cervical examination[2]
- pH assessment of the vaginal sidewalls or fluid pool[3]
- ultrasound examination.

Physical examination is preferred, the last two methods being used when doubt remains on diagnosis.

[2]Digital examination increasing the risk of infection is usually avoided [1].
[3]The pH of the vaginal secretions is generally 4.5-6 whereas amniotic fluid has a pH of 7.1-7.3 [1].

1.4.2 Inferred risks and medical management

At term, 95% of women with PROM are reported to deliver within 28 hours of membrane rupture [26]. For patients with preterm PROM, delivery occurs within 1 week in 55-70% of the cases [27,28]. Rapid assessment and appropriate treatment(s) are crucial.

The diagnosis of PROM is based on accurate knowledge of the associated maternal, fetal and neonatal risks, which include:

- intrauterine infection
- umbilical cord compression
- fetal ascending infection
- complications of prematurity[4].

Depending on fetal presentation and gestational age, the following medical approaches towards management of PROM may be advocated or pursued [1]:

- expectant management[5]
- antibiotic treatment
- labor induction
- cesarean section.

However, numerous controversies still exist regarding the adequate treatment of PROM in both term and preterm births, and no general management guidelines have reached consensus in most cases. Given the potential serious complications resulting from PROM and

[4]Depending on the gestational age, neonatal and postneonatal complications include respiratory distress syndrome (due to pulmonary immaturity), intraventricular hemorrhage, neonatal death, generalized developmental delay, blindness, mental retardation or physical deformation [1].

[5]This usually implies bed rest along with a "watchful waiting" or close monitoring of the patient's and infant's clinical conditions (among other things, assessment of infection risks, fetal heart rate and pulmonary maturity are most often performed).

the limited array of currently available treatments, developing effective prevention methods appears to be of fundamental importance. In this perspective, a better understanding of the different pathological, mechanical and biochemical mechanisms leading to PROM is essential.

1.4.3 Etiology

The causes leading to PROM are multifactorial and poorly understood. They may act individually or in concert. Among them, are:

- pathological factors
- mechanical factors
- biochemical factors.

Pathological factors comprise chronic inflammation and acute infection (such as chorioamnionitis). They cause some local weakening of the tissue and/or the production of the autocrine/paracrine hormones governing the activation of the myometrium responsible for preterm labor [29]. Pathologies such as maternal placental vasculopathy have also been shown to be a separate risk factor for preterm birth, distinct from infection [30].

PROM has also been attributed to purely mechanical factors such as membrane fatigue under repeated uterine contractions [31] or local membrane stress concentration. Stresses may be generated locally:

- in shear along the uterine wall from preterm contractions and/or by partial delamination of the chorionic layer from the amnion or the decidua[6]
- by membrane prolapse along the cervical inner canal

[6]Separation of amnion from choriodecidua might be integral part of the normal event sequence resulting in membrane rupture at term, as suggested by a study published this month [32].

- by abnormally high amniotic fluid pressure[7].

Biochemical factors mainly refer to the enzymatic and hormonal processes resulting in partial disruption of the ECM components, membrane weakening, and subsequent tissue failure. Most studies available have focused on the possible correlations between collagen content and membrane rupture. The biochemical integrity of soft tissue relies on a subtle equilibrium between collagen synthesis and degradation troughout pregnancy. At term, preceding the onset of labor, this balance is thought to shift towards proteolytic degradation of the collagen fibrils, resulting in decreased collagen content and membrane rupture[8]. Similar explanations have been proposed for PROM, including increased collagenolytic activity, reduced collagen synthesis, or altered collagen structure [3]. These biochemical changes might be dictated by:

- abnormal genetic expression [43,44]
- hormonal regulation [45–48]
- nutritional deficiencies [3]
- local infection [49].

However, despite substantial investigation into the etiologies of PROM, no direct correlation has yet been established between PROM and the mechanical and biochemical factors succinctly reviewed in this chapter. A better understanding of the biochemical processes involved with tissue growth, remodeling and degradation is needed. Further, the comprehension of its intrinsic mechanical behavior in relation to its biochemistry is crucial for understanding the "cascade" of microstructural mechanisms governing PROM.

The aim of this study is to characterize the mechanical response and biochemical content of the CA membrane in vitro, through uniaxial and biaxial testing on the one hand, and

[7]Hydroamnios which is a pathology characterized by excess amniotic fluid, may be associated with PROM [33,34]. The amniotic fluid pressure of women presenting hydramnios has been found to be ~40% higher than that of healthy patients [35].

[8]One large study [36] amid other contradictory results [37–42] tends to confirm this hypothesis.

measurements of the hydration levels, collagen and sulftated GAG contents, on the other hand.

Chapter 2

Experiments

This chapter will focus on the experimental protocols for handling and testing of the chorioamnionic (CA) membrane. The membrane was tested for its mechanical and biochemical properties; thickness measurements were also obtained on both the amnion and chorion layers. Two types of mechanical testing were devised and implemented: uniaxial tensile tests on a single amnion layer (load-unload, creep, stress relaxation), and biaxial pressurized bulge tests on chorioamnion. In addition, biochemical assays measured the hydration level, the collagen and sulfated glycosaminoglycan (GAG) content (per dry weight of tissue), and the collagen extractability of the fetal tissue. A histological examination of the membranes was also performed to detect any possible sign of infection.

2.1 Tissue collection and preparation

CA samples were obtained from the Tufts-New England Medical Center (Division of Maternal Fetal Medicine, Boston, Massachusetts). Patients consenting for the study[1] were unlabored women undergoing elective cesarean section at term. An approximate 20×20 cm^2 section of

[1] Consent of the patient was obtained according to a protocol approved by the Institutional Review Board at the New England Medical Center. The details of the clinical variables collected for each patient can be found in Appendix A.

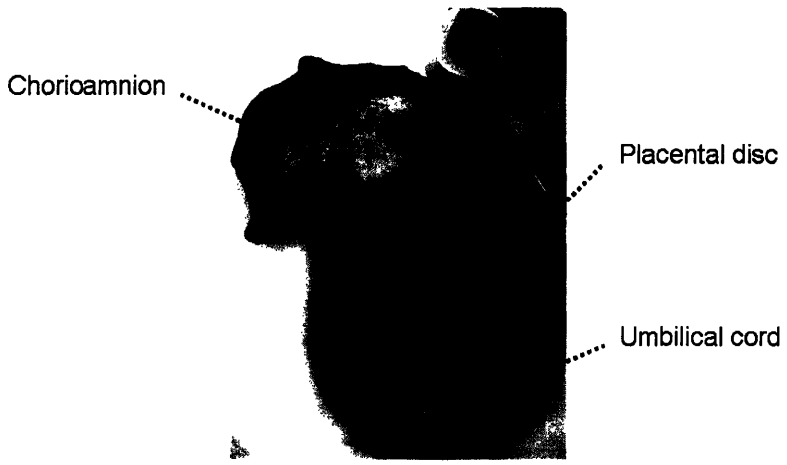

Figure 2-1: Chorioamnionic membrane and placental disc collected after delivery.

the membrane was carefully cut with surgical scissors, excluding the region of the placental disc (Figure 2-1); the specimen was then immersed in standard saline solution and kept on ice. An approximate 2×5 cm^2 strip was saved for histology[2]; the remaining part was transferred to the laboratory, rinsed in saline and carefully cut into three 9×9 cm^2 pieces for uniaxial, biaxial, and biochemical testing respectively. For biaxial testing, the membrane was left intact and tested as a single chorioamnionic layer. For uniaxial tension tests and biochemical analysis, the selected membrane pieces were separated apart into individual amnion and chorion components by means of gentle traction (see Appendix B for details). All testing was performed at room temperature within a few hours following delivery[3].

[2]The histology slides were stained hemotoxylin and eosin in the standard manner. They were then reviewed with an attending pathologist at the New England Medical Center.

[3]The temperature, measured for each series of testing, oscillated between 21°C and 25°C.

2.2 Uniaxial tensile test

2.2.1 Materials and methods

Following separation from chorion, the amnion sample was allowed to recover for a few hours in saline solution[4]. The specimen was then cut into approximate 6 × 25 mm^2 strips using a rotary cutter[5]. The samples were clamped between two aluminum grips, specifically designed for soft-tissue gripping[6], and loaded vertically into a universal material testing machine (Zwick Z2.5/TSIS, Ulm, Germany). The tissue was kept hydrated during the entire handling process and placed in solution within a transparent fluid box during testing (Figure 2-2). Specific protocols can be found in Appendix B.

2.2.2 Measurements

Force (F) and displacement (ΔL) were recorded every 100 ms along the vertical direction of stretch via a 20 N load cell; the initial gauge length (L_0) was set at 10 mm (Figure 2-3). The tissue deformation in the transverse direction was tracked using a digital image correlation technique (VIC-2D version 4.4.0) with a QImaging Retiga 1300 CCD camera (Figure 2-2). Images, taken every 100 ms, were automatically correlated to the corresponding tensile "force-displacement" output from the Zwick Test Control software.

Three distinct tensile tests were performed:

- load-unload cycles
- creep
- stress relaxation

Three specimens were used per test, to get relevant statistical results for each patient. The tests' definition is detailed hereafter for 6 mm wide samples.

[4]The specimen slightly stretched during the separation process was found to approximatively recover its original shape after sitting two to three hours in solution.

[5]After numerous tries of different cutting tools (including scissors and cutting press), the rotary cutter turned out to be most appropriate to ensure minimum shear stress while cutting and smooth regular edges.

[6]The fixtures were made at the MIT Central Machine Shop and coated with sandpaper to prevent slipping.

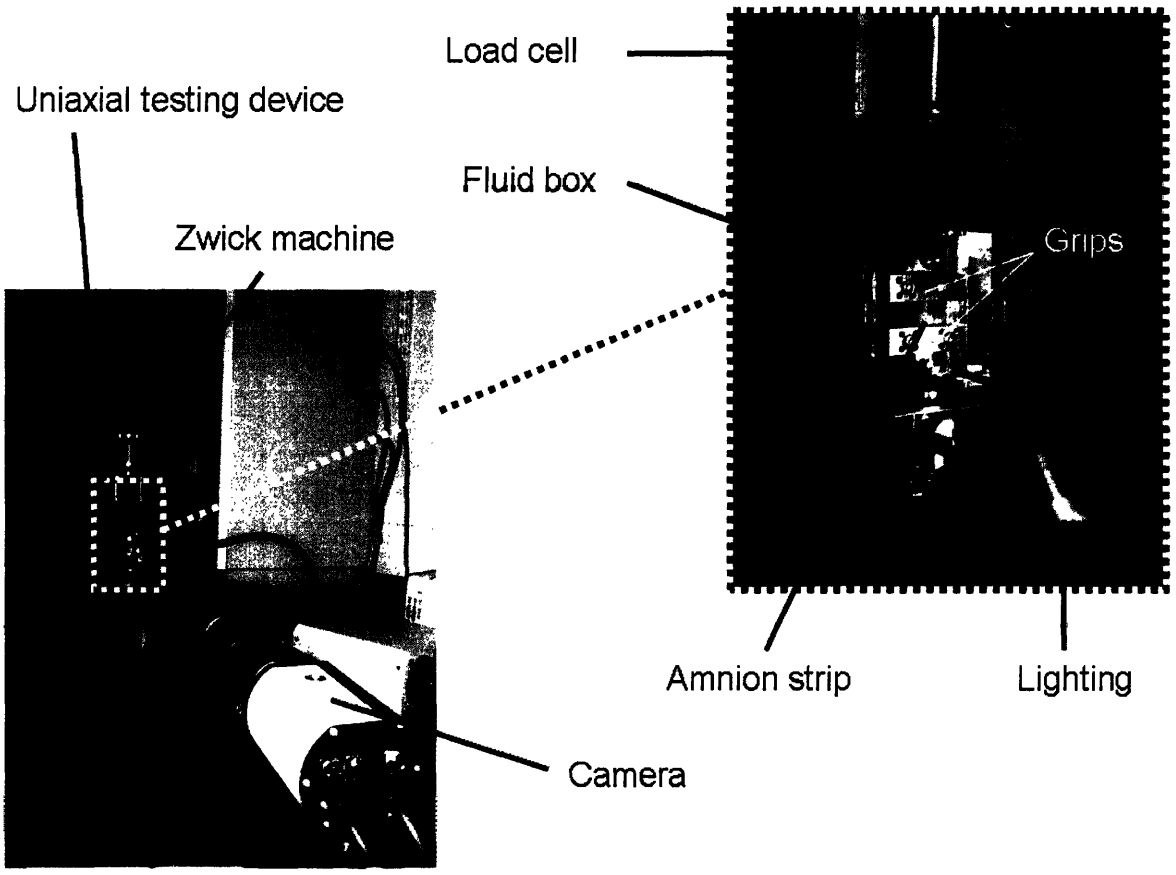

Figure 2-2: Uniaxial testing apparatus.

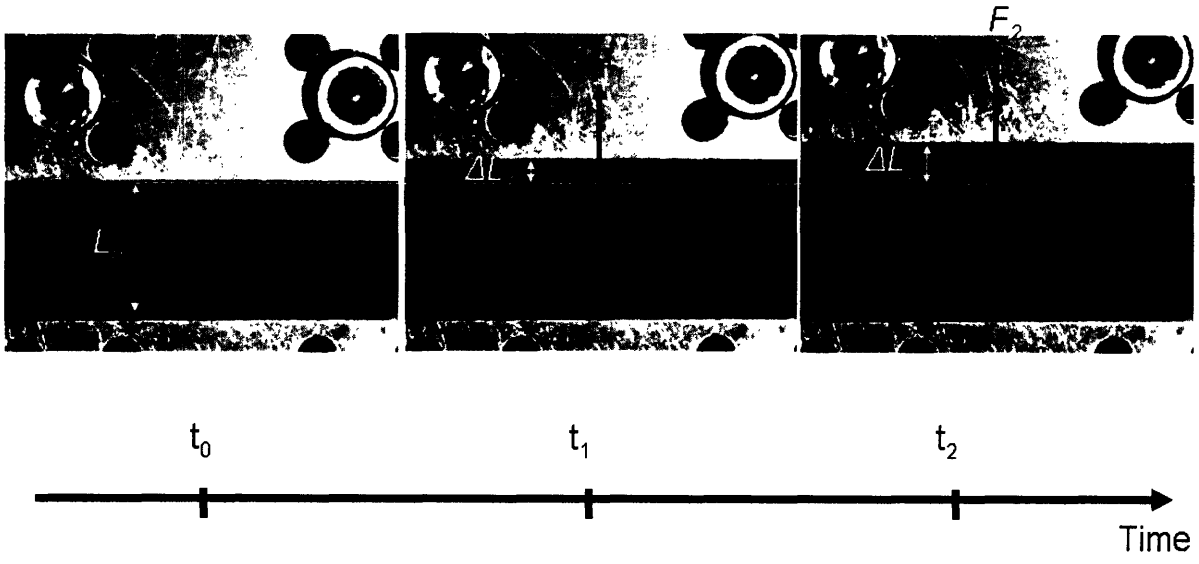

Figure 2-3: Force (F) and grip displacement (ΔL) as recorded along the vertical tensile direction.

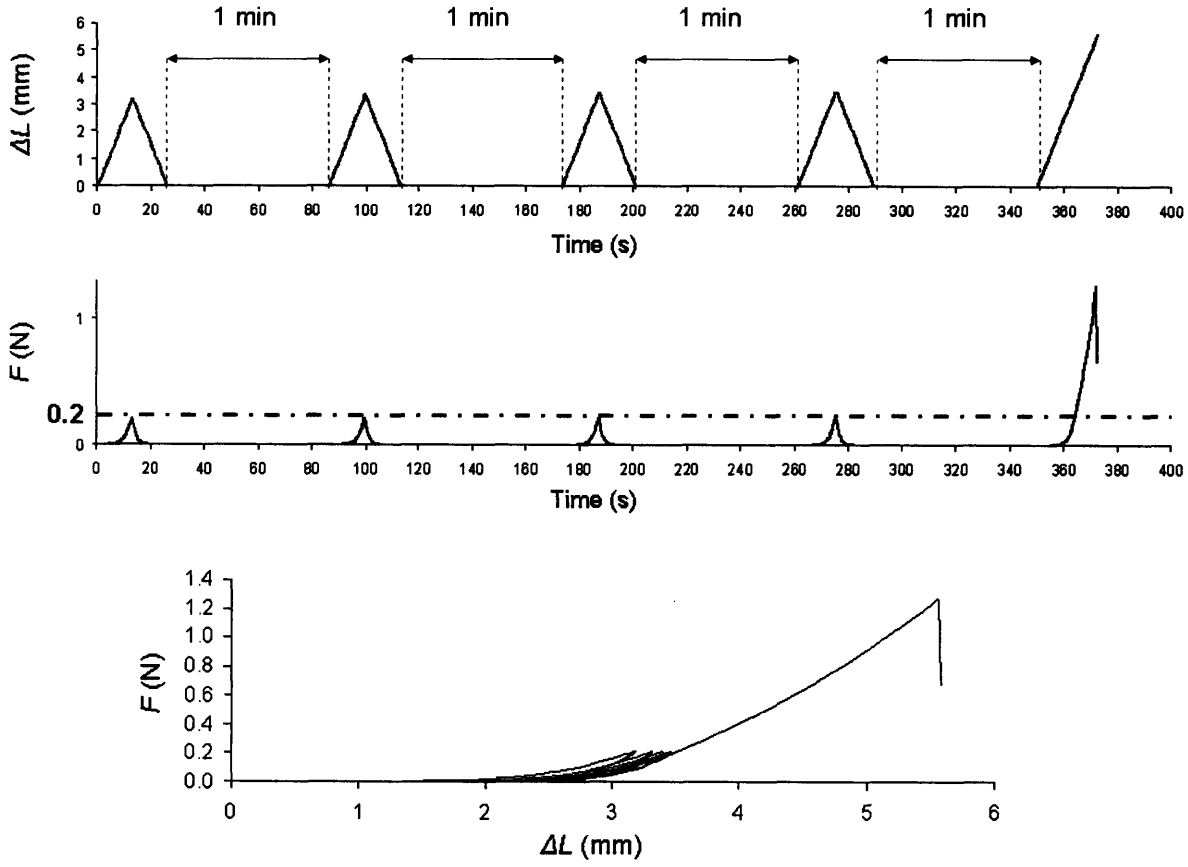

Figure 2-4: Uniaxial load-unload cycle definition.

Load-unload cycles

The specimens were subjected to a set of four load-unload cycles, at a displacement rate of 0.25 mm/s, to the same 0.2 N peak force[7]. The recovery time between two successive cycles was set at one minute. The specimens were finally strained to failure (Figure 2-4).

[7]The 0.2N peak value corresponded to a 15-50% strain level which is within the strain range experienced in vivo (see Section 3.5).

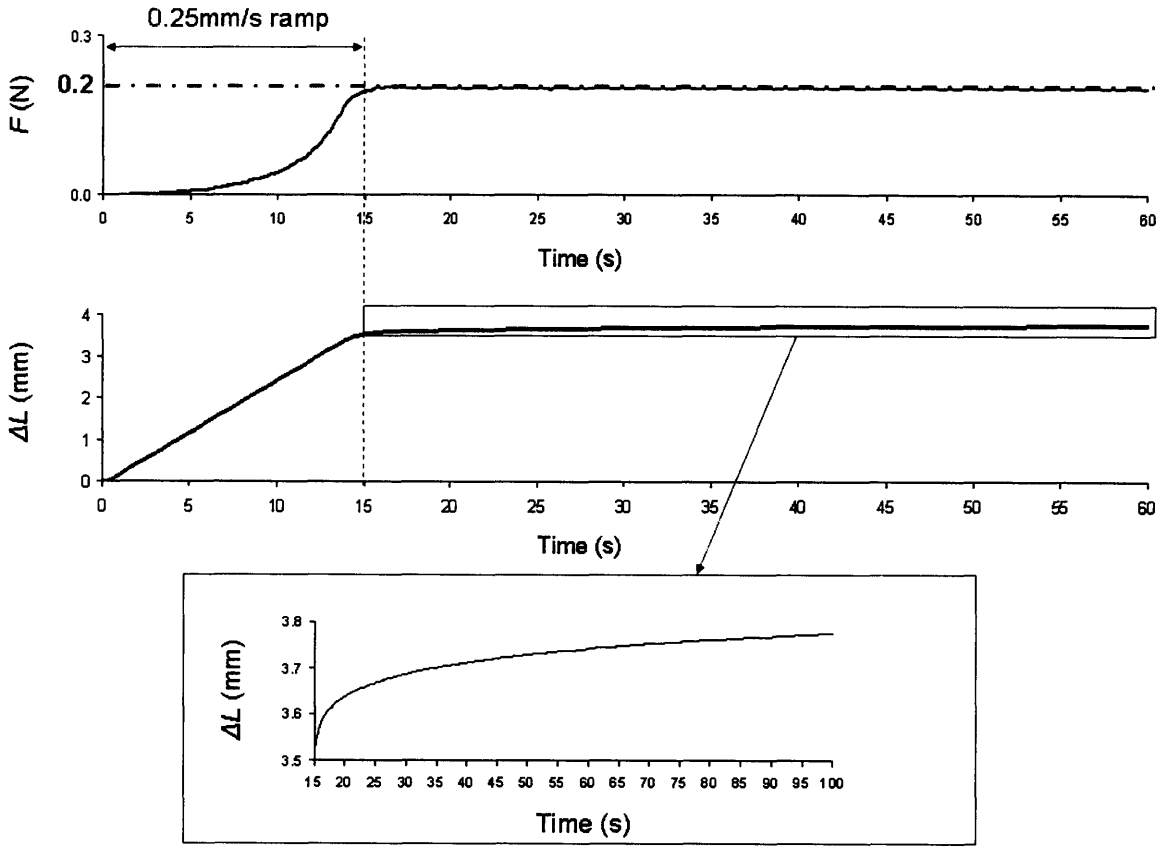

Figure 2-5: Uniaxial creep test definition over the first 100 seconds.

Creep

The samples were stretched up to 0.2 N at a 0.25 mm/s strain rate, followed by a 20-60 min. force hold[8] (Figure 2-5). Unloading was then performed at the same 0.25 mm/s strain rate and the specimens were allowed to recover for one minute before being stretched up to failure.

[8]The creep time was set at 20 minutes for the first two specimens and 60 minutes for the last one.

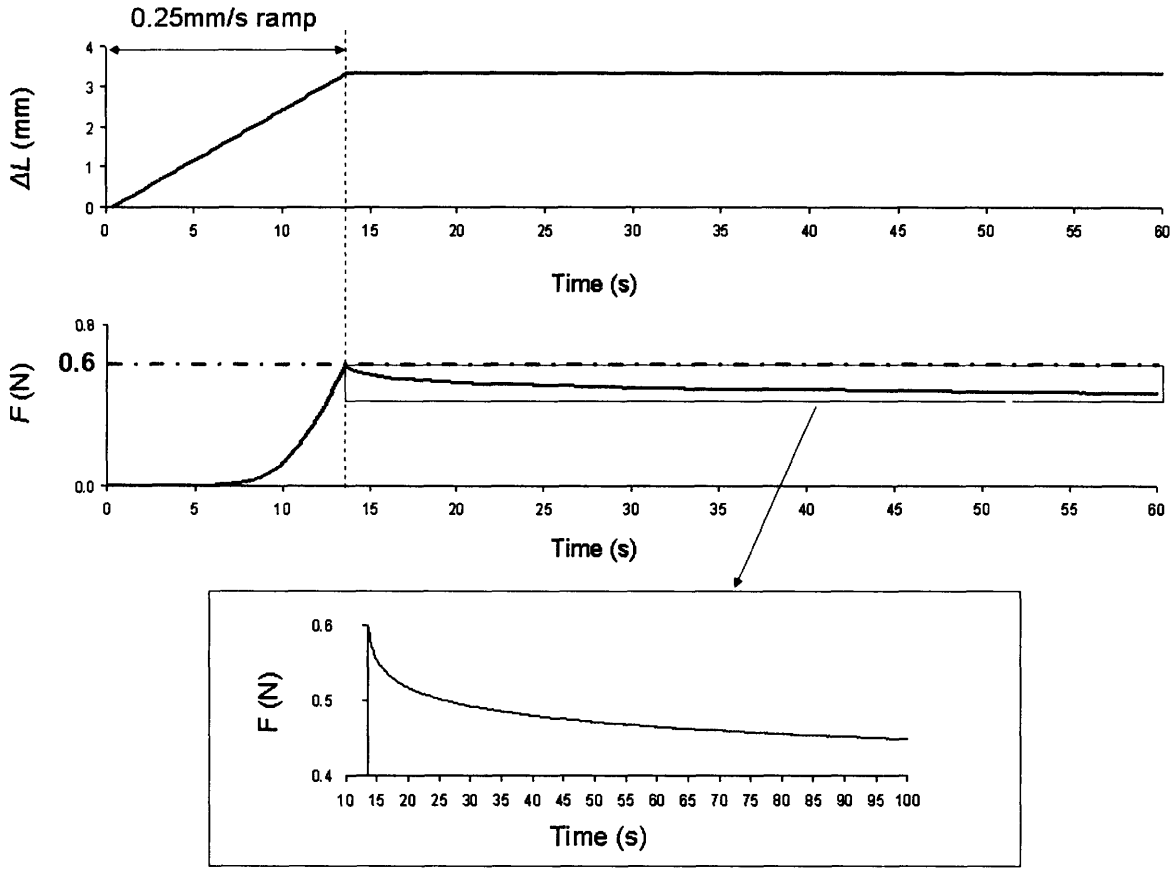

Figure 2-6: Uniaxial stress relaxation definition over the first 100 seconds.

Stress relaxation

The specimens were loaded up to the same peak force of 0.6 N[9] at a 0.25 mm/s displacement rate, before relaxing 20 minutes for the first two tests and over 24 hours for the last one (Figure 2-6). All specimens were subsequently unloaded at a rate of 0.25 mm/s. Following a one minute recovery time, they were finally strained up to failure.

[9]Given the strong peak stress dependence of the tissue's relaxation response observed in a preliminary investigation, relaxation tests were defined starting from the same peak force and not from the same peak displacement. Relaxation responses were found to be reproducible.

2.2.3 Comments

The amnion is a very thin slippery membrane which grows and develops in a fluid environment. Because of its delicate nature, the tissue damages easily during handling, especially while in contact with the grips. Therefore, its handling and loading require great care (see Appendix B for more details). The following factors must be taken into account to obtain reliable results:

- constant hydration
- proper gripping
- adjustment of specimen at "initial configuration".

Hydrating the membrane is essential, not only to avoid tissue damage but also to prevent the membrane from rolling upon itself. Proper gripping ensures that the specimen is correctly placed at the grip center and perfectly aligned with the vertical direction of test. The adjustment of the specimen at "initial configuration" is another significant concern. Making sure that the specimen is neither pre-stretched nor slack before test initiation is of crucial importance to secure valid reproducible results. To address the issue, the bottom grip was tightened after the specimen had been loaded into the machine (see Appendix B.3).

Finally, a technical difficulty was encountered: the load cell occasionally showed signs of instability after three to ten hours of testing. As a consequence, stress relaxation tests over 24 hours could not always be carried out successfully[10].

[10]It could never be determined with 100% certainty whether the small force fluctuations (± 4 mN) measured after more than three hours of testing arose from internal electronic machine problems or environmental perturbations (such as temperature variations, power fluctuations or external mechanical vibrations). The power supply and the temperature regulation were checked. The DC card of the Zwick machine was also changed. As a result, the long-term force fluctuation problem was alleviated, even though not completely sorted out.

2.3 Pressurized bulge test

2.3.1 Apparatus and methods

The apparatus designed for biaxial testing is shown in Figure 2-7. The mechanical drawings of the device parts are included in Appendix D.

The CA membrane was fastened to a 54 mm diameter hollow acrylic cylinder with an O-Ring and stainless steel sleeve whose diameter was adjusted to tighten the membrane. The cylinder was then immersed in saline solution within a 30 × 20 × 15 cm^3 transparent acrylic fluid box, and connected to an upper tank whose incremental raising was used to control pressure.

The membrane was submitted to discrete pressure increases by 500-2000 Pa increments until failure occurred. Each pressure step was held for ten minutes. The pressure level and stability within the cylindrical cavity were tracked by a 5 psi range pressure transducer, and the deflection of the pressurized membrane was recorded by a digital camera at a 1 Hz rate.

Further details concerning the pressurized bulge test protocol can be found in Appendix B.2.

2.3.2 Measurements

Pressure control

The pressure level was directly controlled through the height difference between the saline bath and the upper tank, a pressure increase Δp related to a tank lifting ΔH by the fluid statics Equation 2.1

$$\Delta p = \rho_{water} \times g \times \Delta H \tag{2.1}$$

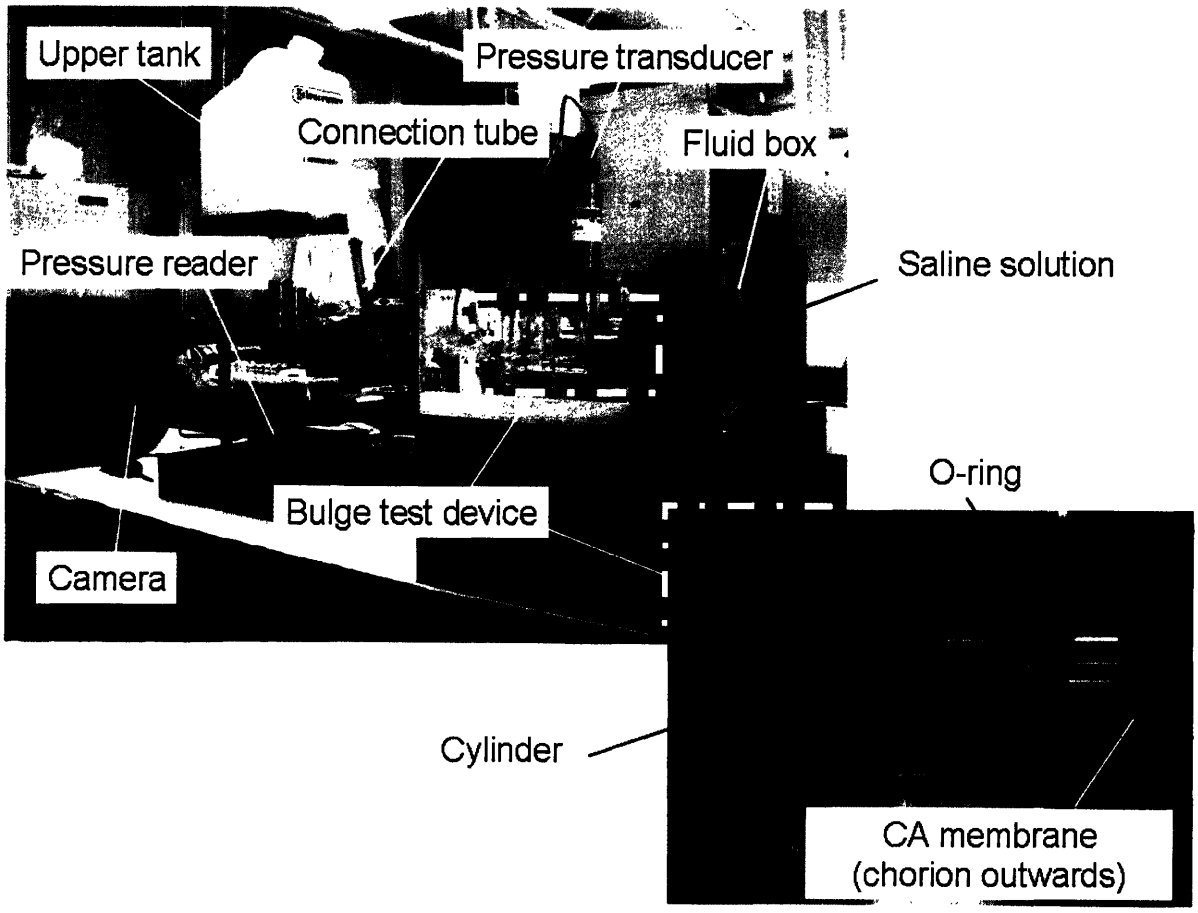

Figure 2-7: Pictures of pressurized bulge test apparatus.

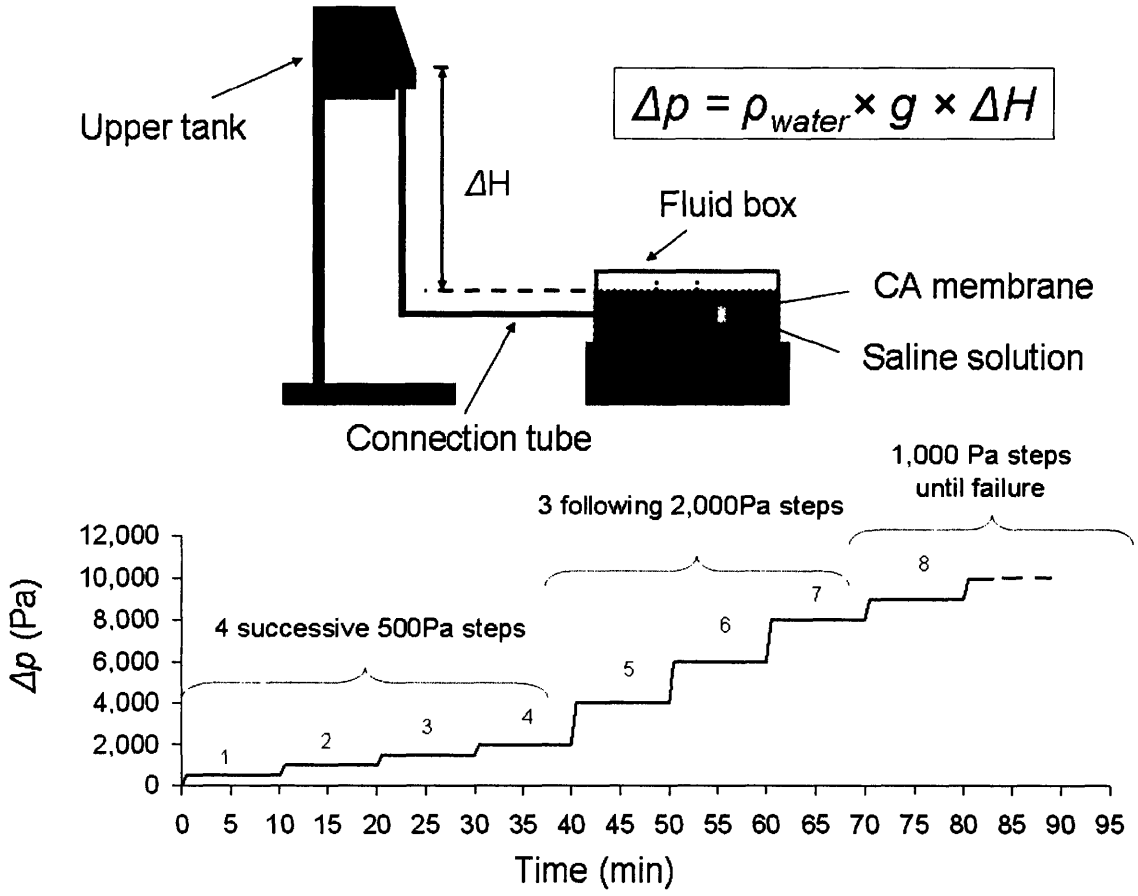

Figure 2-8: Schematic illustration of pressurized bulge test device and protocol.

where ρ_{water} is the volume mass of water[11] at 20°C (i.e. 1000 Kg.m^{-3}) and g, the gravity (taken as 9.8 m.s^{-2}).

The tank was therefore manually lifted by 5.1 cm, 10.2 cm or 20.4 cm to obtain the desired pressure increases by 500 Pa, 1000 Pa or 2000 Pa respectively (Figure 2-8). The pressure values measured experimentally with the pressure transducer were found to be in very good agreement with the above theoretical values[12].

[11]The volume mass involved in reality is that of the saline solution which was approximated to that of pure water.

[12]The pressure levels measured at equilibrium by the transducer deviated by less than 5% from the expected ones.

The samples, initially stress free, were first submitted to four successive 500 Pa pressure increase steps in an effort to capture the large tissue deformation at low pressure ranges. The next three pressure increments were set to 2000 Pa (the tissue being significantly stiffer at higher pressure levels). Finally, the behavior of the tissue to failure was tracked through 1000 Pa pressure steps (Figure 2-8). The time needed for pressure to equilibrate after each new pressure increase was 5-20 seconds: the pressure increments were therefore considered as *quasi-instantaneous*[13].

Deflection profile

The deflection profile tracked by the camera every second was retrieved through image analysis, using commercial software MATLAB 7.0.4. The main analyis steps are shown in Figure 2-9. The MATLAB programs written for the image analysis can be found in Appendix E. The image size was 1280 × 1024 pixels, thereby providing a camera resolution of 0.07-0.1mm (i.e. less than 1% of the deflection magnitude).

2.3.3 Comments

The handling of the tissue, even though less "tricky" than uniaxial testing specimen handling, does require some careful adjustments. In particular, the following considerations are important:

- the specimen must neither be stretched nor damaged by the ring during tightening
- no fluid pressure must be applied to the membrane before starting the test (in other words, the fluid pressure inside the cylindrical cavity must equal that in the surrounding bath)
- the cylinder must be properly sealed to avoid any leakage during pressurization.

[13] A few seconds are negligible when compared to the overall ten-minute duration of each step.

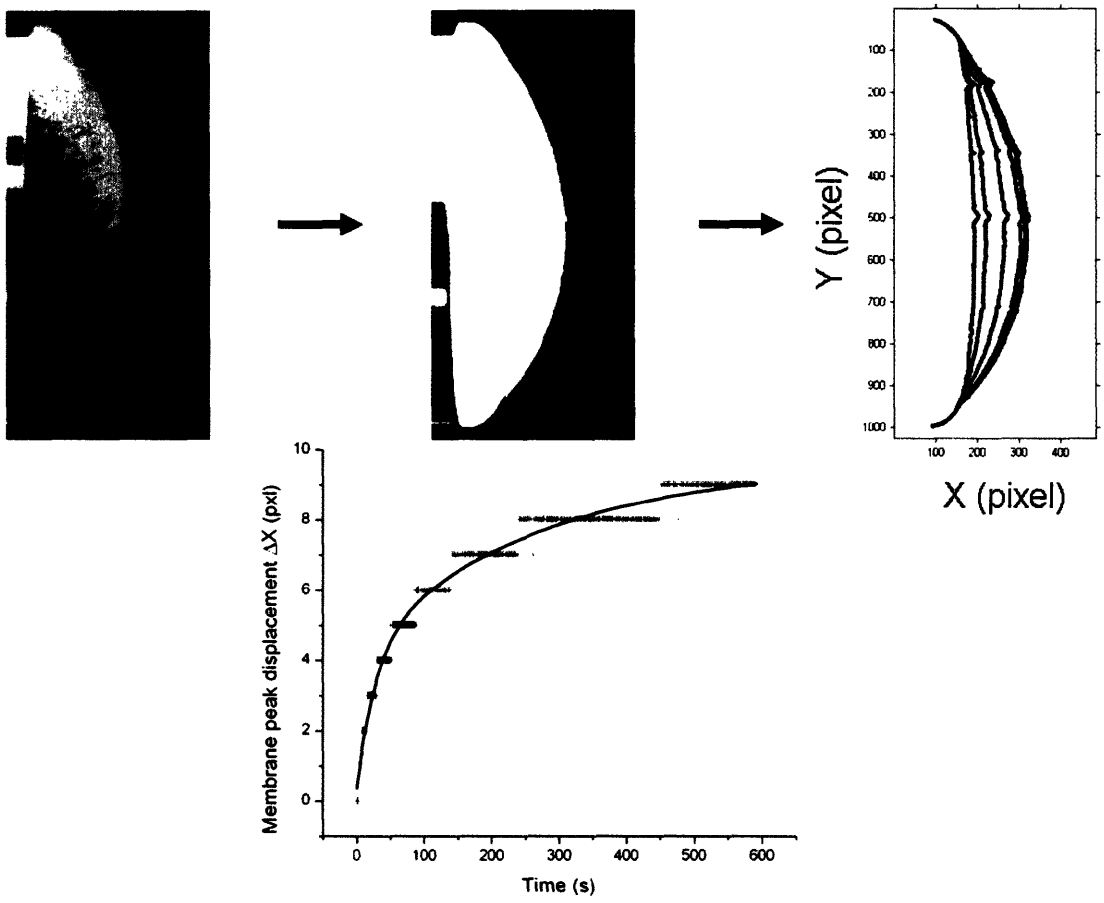

Figure 2-9: Membrane deflection profile analysis through MATLAB. Profile peak tracked as a function of time at any given pressure step.

2.4 Biochemical testing

Biochemical testing was performed on chorion and amnion separately, following a protocol developed by Myers [50]. Five biochemical data sets were obtained per membrane:

- water content
- amnion/chorion mass ratio
- collagen content (per dry tissue weight)
- collagen extractability
- sulfated proteoglycan content (per dry tissue weight)

The guidelines of the experimental procedure are shown in Figure 2-10. Further details concerning the biochemical assays are given in Appendix C.

2.5 Thickness measurement

The amnion and chorion layers were separated and cut into approximate 9×25 mm^2 strips. Three strips were selected per layer. The former were properly dried on lab tissue and placed between two microplates. The thickness of the "sandwiched structure" was then measured using Fischer magnetic induction probe ETA3 providing an accuracy of 1 μm. The details of the protocol can be found in Appendix B.4.

2.6 Protocol summary

Figure 2-11 summarizes the main steps involved in the membrane protocols.

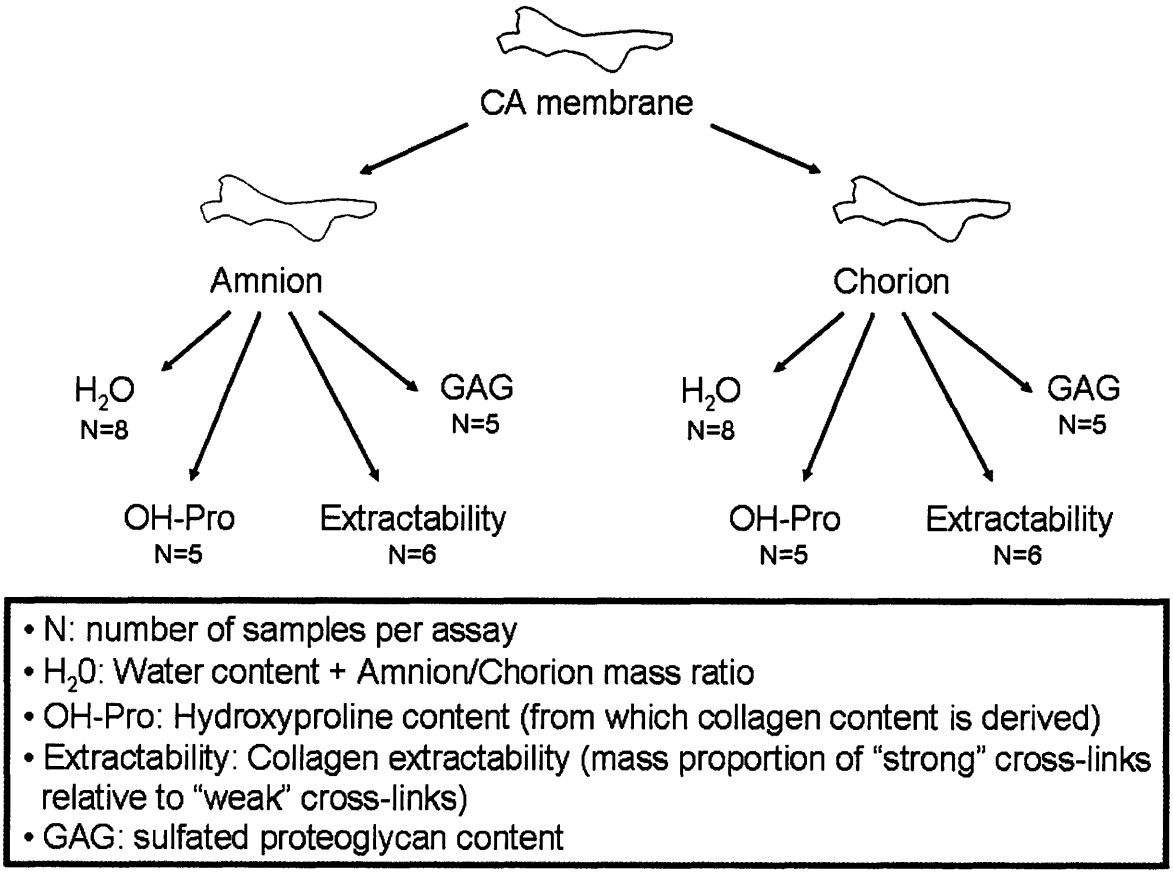

Figure 2-10: Summary of biochemical assay protocol.

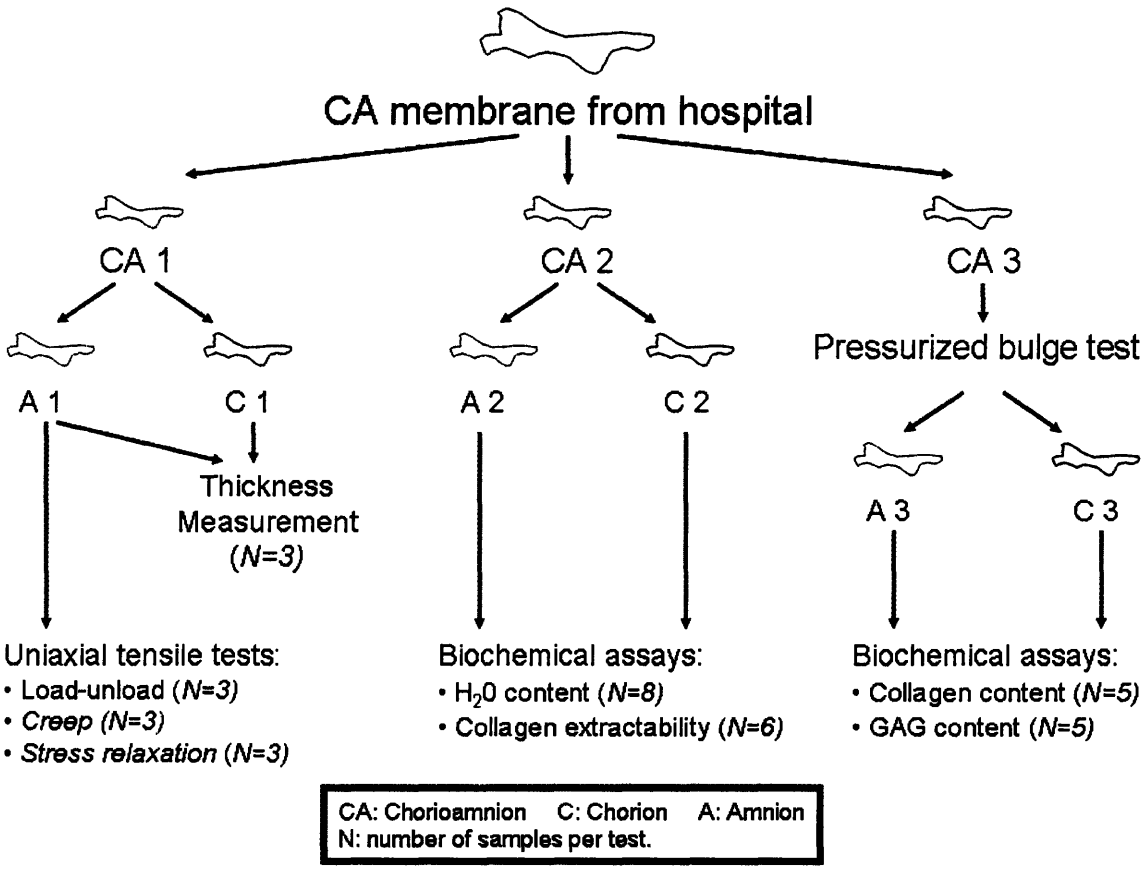

Figure 2-11: Summary of the membrane protocols.

Chapter 3

Results

The experimental results presented in this chapter were obtained from seven patients who had an elective cesarean section at 39 weeks gestation[1]. The results were compared, whenever possible, to those existing in the literature.

3.1 Histological studies

The histology slides of the fetal membranes (Figure 3-1) were reviewed at the New England Medical Center, and no histological evidence of chorioamnionitis was noted.

3.2 Membrane thickness

Table 3.1 summarizes the membrane thickness measurements obtained from the protocol developed in this study (Appendix B.4). Because of the thin and delicate nature of the fetal membranes, significant variations in the measurement[2] were observed and an accurate thickness assessment was difficult to obtain. However, the measurement procedure was

[1]The patients were unlabored. The cesarean sections were performed because either the patient declined a vaginal birth after cesarean (N=5) or a previous myomectomy was performed (N=2). The cervix was dilated less than 1 cm in all cases. There was no clinical evidence of chorioamnionitis.

[2]Measurement uncertainties mainly came from: intrinsic tissue inhomogeneities (especially for the chorion), amnion-chorion separation irregularities (the intermediate spongy layer, usually part of the amnion layer, might have, in some cases, remained partly attached to the chorion and therefore been included in the chorion thickness measurement) and other protocol details such as the tissue drying level and its appropriate squeezing prior to measurement.

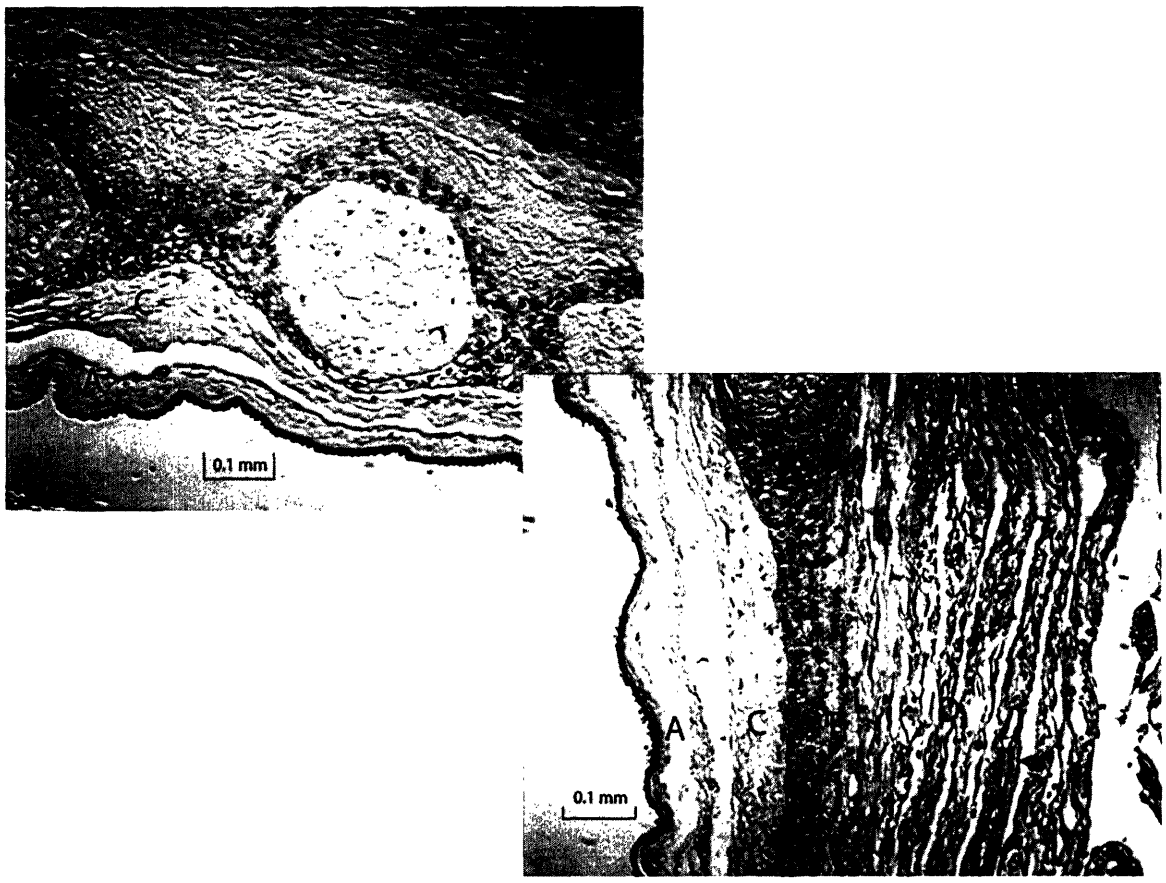

Figure 3-1: Histological cross-sections from one typical CA specimen, showing the amnion layer (A), the chorion layer (C) with its trophoblast layer (T), and part of the decidua (D). The histological studies were performed by Dr. Michael House at the New-England Medical Center.

	Measured thickness	Halaburt et al. [39]	Oxlund et al. [9]
Number of patients	7	4	6
Amnion thickness (μm)	53 ±28	60 ±3.5	47 ±4
Chorion thickness (μm)	247 ±50	318 ±34.2	185 ±15

Table 3.1: Amnion and chorion thickness measurements.

	Measured hydration	Halaburt et al. [39]	Meinert et al. [14]
Number of patients	7	26	9
A water content (%)	87 ±4.2	87.5 ±2.6	86
C water content (%)	89.9 ±1	85.8 ±1	86
A/C wet mass ratio (%)	10.2 ±2.2	-	-
A/C dry mass ratio (%)	13.5 ±1.7	-	-

Table 3.2: Amnion and chorion hydration level and mass ratios. The mass ratios are based on 5 patients only. No measurement uncertainty was provided by Meinert et al.

found reproducible and the results derived were consistent with those published in earlier studies [9,39].

3.3 Biochemical testing

This section reports measurements for the hydration level, the sulfated glycosaminoglycan and collagen contents (per dry weight), and the collagen extractability of chorion (C) and amnion (A). Results are compared with those in the literature.

3.3.1 Water content and amnion/chorion mass ratios

The hydration level of both amnion and chorion was consistently 88% (±5). These measurements were in good agreement with previous results [14,39]. The amnion/chorion (A/C) dry and wet mass ratios, which have not been assessed in the past, were also determined (Table 3.2).

	Collagen content	[14] 2001	[42] 2000	[41] 1997	[39] 1989
Number of patients	7	9	12	25	29
A collagen content (μg/mg dry weight)	419 ±73	382 ±23	357 ±68	525 (336-702)	336 ±54
C collagen content (μg/mg dry weight)	155 ±29	122 ±8	-	-	145 ±38

Table 3.3: Amnion and chorion collagen contents.

3.3.2 Sulfated glycosaminoglycan content

The average sulfated glycosaminoglycan contents of amnion and chorion were measured to be 213 (±31) μg/mg dry tissue weight and 188 (±36) μg/mg dry tissue weight, respectively. These results, however, could not be directly compared to the literature, since most previous studies reporting measurements for the proteoglycan content of fetal membranes mainly focused on specific families of proteoglycans or glycosaminoglycans (such as decorin, biglycan and hyaluronan), or used different characterization methods like alcian blue precipitation or electrophoretic separation [14,51].

3.3.3 Collagen content - Collagen extractability

Several earlier studies [14,38,39,41,42] evaluated the collagen content of amnion (A), chorion (C), and/or chorioamnion (CA), from the tissue hydroxyproline content. Results in the literature and results obtained in this study are shown in Table 3.3. It was confirmed that the amnion has more than twice the amount of collagen when compared to the chorion.

The collagen extractability level, defined in % as the proportion of relatively weaker crosslinked collagen fibers (see Appendix C.6 for details), was measured to be 56±8 % for the amnion and 74 ±6 % for the chorion. The significantly lower extractability level measured for the amnion is in accordance with the substantial difference in stiffness noted experimentally between the two layers [9,52].

3.4 Mechanical testing

The aim of this section is to present the main experimental results obtained from mechanical testing and to compare them with those existing in the literature. Unlike the chorion, for which there exist limited mechanical studies[3] [9,52], the amnion layer (separated or not from the chorionic layer) has been the focus of number of mechanical investigations. Uniaxial tensile tests [9,52,53,63], biaxial puncture tests [54,55], and pressurized bulge tests [56–61] were among the most commonly performed tests.

3.4.1 Uniaxial tensile tests

Results

The results provided in this section are based on tests performed on membrane specimens from one representative patient (Figures 3-2, 3-3 and 3-4). For each type of test, the three experimental curves along with their average curve (which will be used in the modeling part) are presented. The amnion thickness, used for the stress calculation, was measured to be 43.3 μm.

The viscoelastic response of the tissue was found to be strongly non linear. The average stress relaxation and creep responses were fitted to a second order exponential decay function of the form:

$$f(t) = A_1 e^{-\frac{t}{t_1}} + A_2 e^{-\frac{t}{t_2}} + y_0 \tag{3.1}$$

The corresponding sets of time constants associated with the creep ($t_1 = 35.1\ s$, $t_2 = 497.3\ s$) and stress relaxation ($t_1 = 22.3\ s$, $t_2 = 415.3\ s$) responses were found to be comparable (Figures 3-5, 3-6).

[3]Several attempts were made, using the uniaxial tensile test apparatus, but tissue damage could hardly be prevented and the results were found non-reproducible.

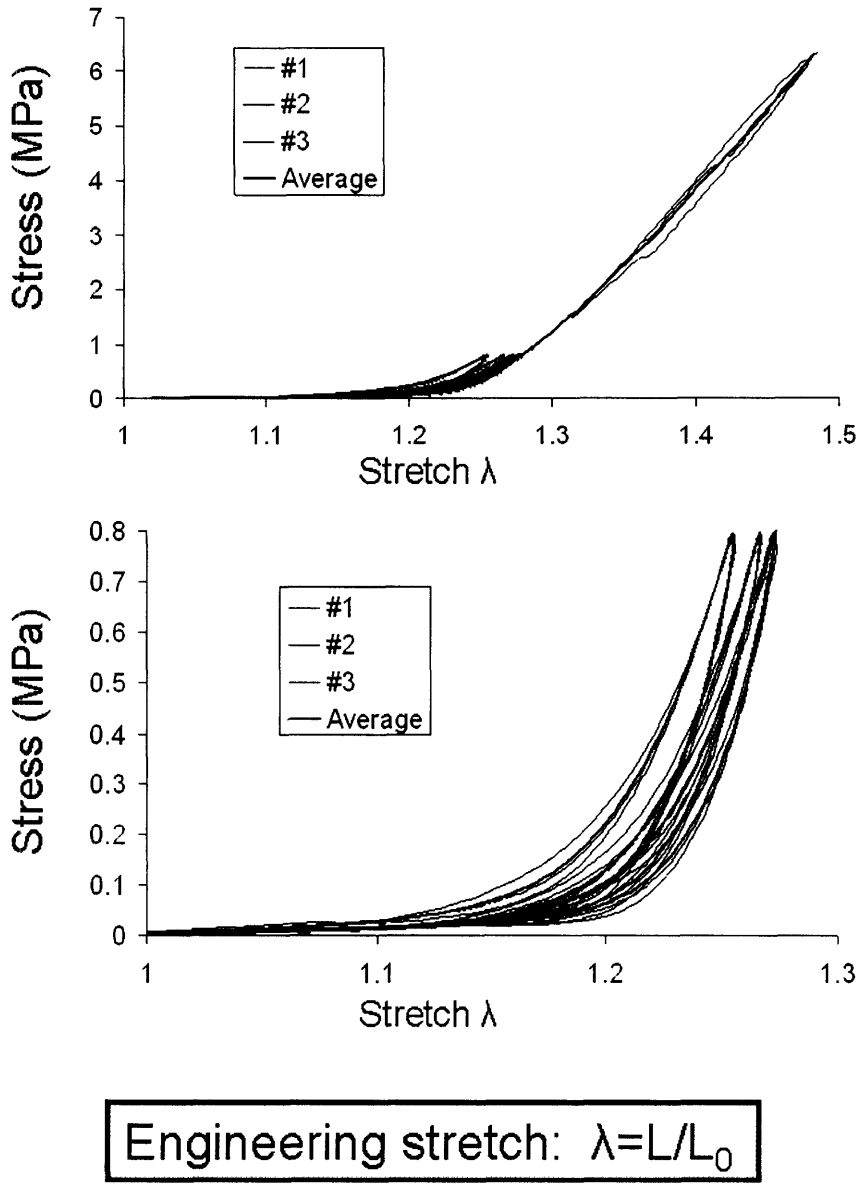

Figure 3-2: Uniaxial load-unload cycles from one typical patient. The average curve is shown in red.

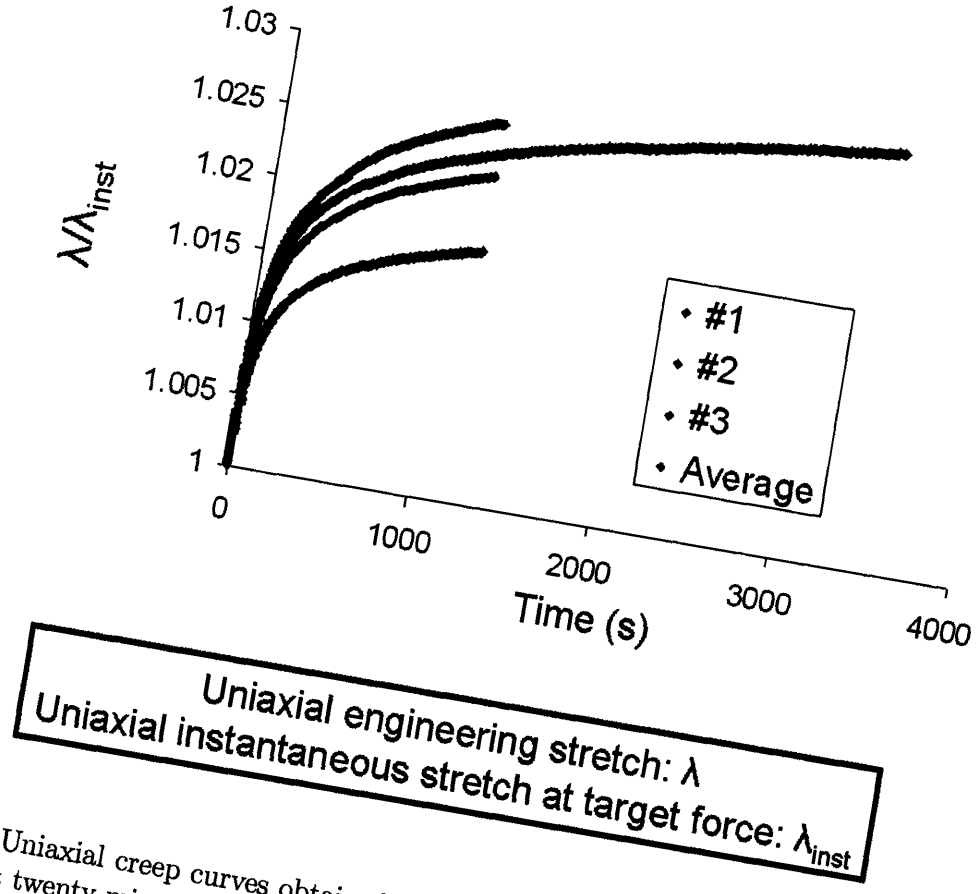

Figure 3-3: Uniaxial creep curves obtained from one typical patient. The average response over the first twenty minutes is shown in red.

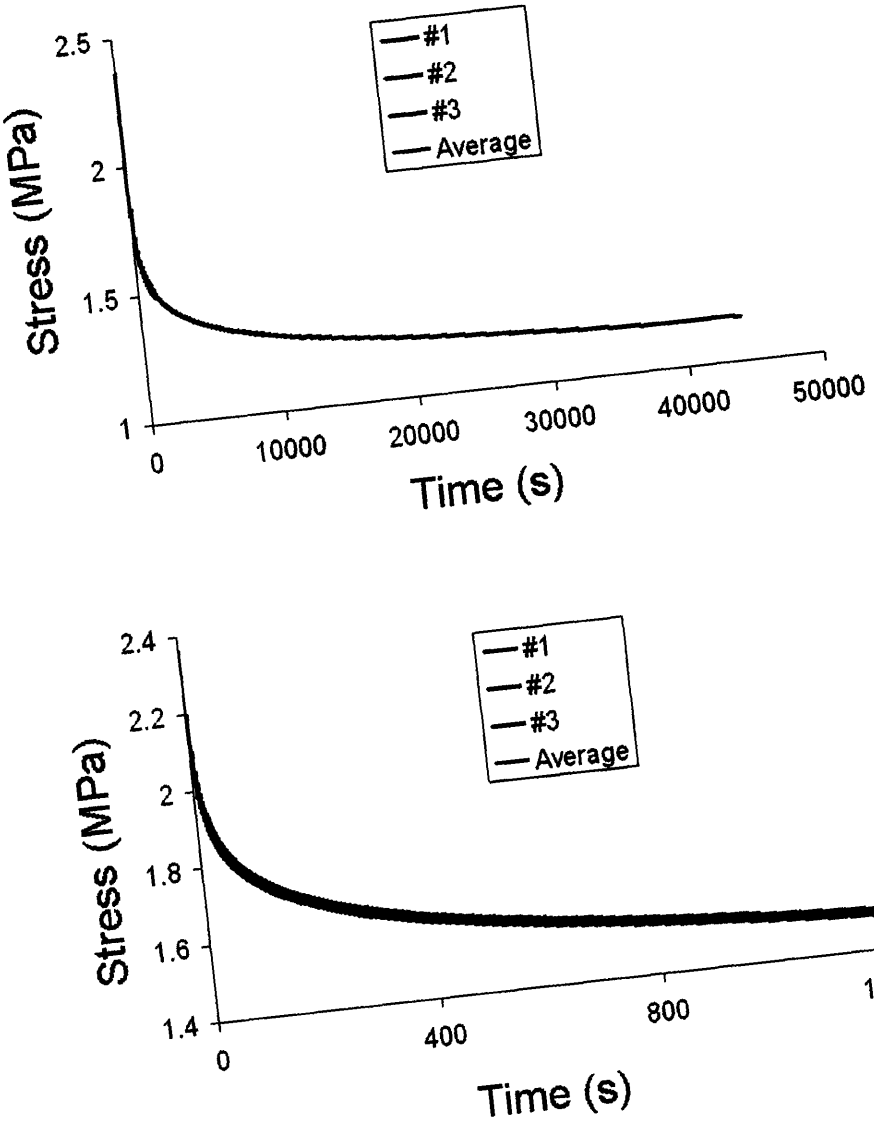

Figure 3-4: Uniaxial stress relaxation curves from one typical patient. The average response over the first 20 minutes is shown in red.

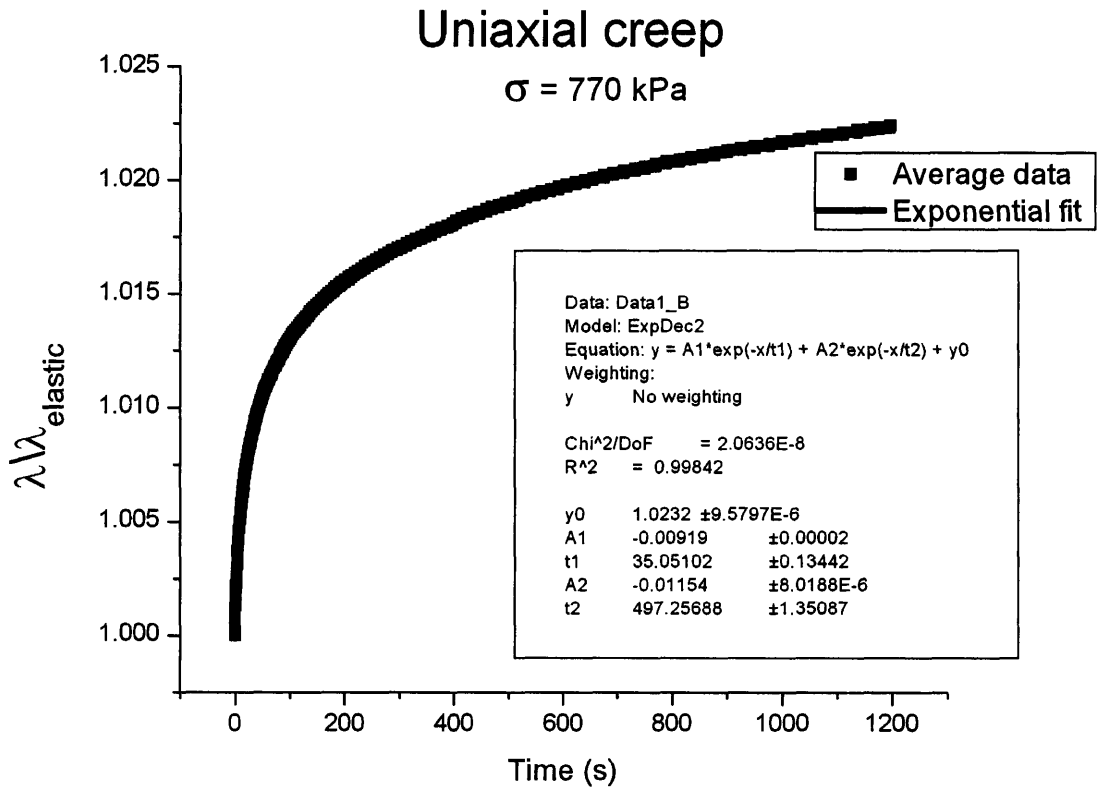

Figure 3-5: Uniaxial average creep response from one typical patient fitted to an exponential decay function.

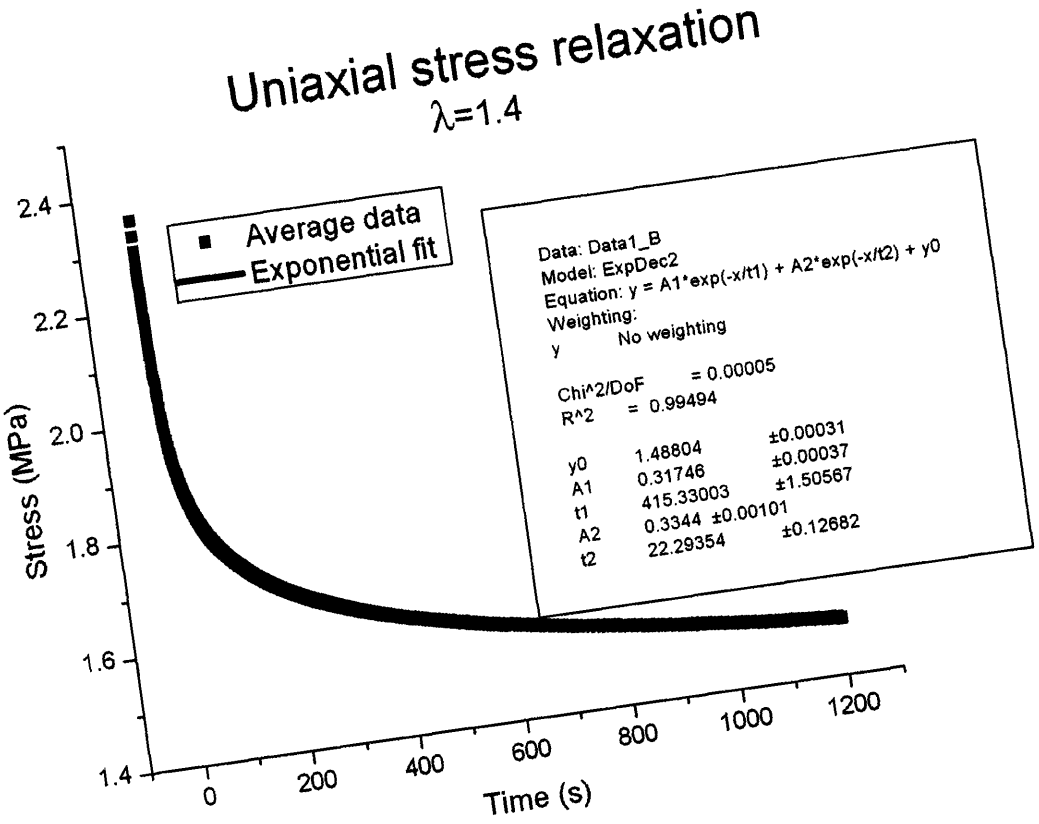

Figure 3-6: Uniaxial average stress relaxation response from one typical patient fitted to an exponential decay function.

	Present study	Helmig et al. [52]	Oyen et al. [53]
Number of patients	7	6	6
ϵ_f (%)	45.5 ±9.8	-	38.4 ±2.7[3]
σ_f (MPa)	3.6 ±1.4	6.6 (4.2-10)	5.2 ±2.1
E_f (MPa)	19.2 ±4	29.5 (17.1-43.3)	23.1 ±6.3

Table 3.4: Comparison of parameters from the uniaxial strain-to-failure curves. Stress computation is based on a 50 micrometer thickness.

Comparison with literature

Most previous studies focused on the uniaxial strain-to-failure response of the amnion. Under uniaxial tension, the amnion layer exhibits the same basic force-stretch pattern as that of a collagen fiber [62], characterized by an initial "stress-free" response followed by a significant increase in stiffness (Figure 3-7). The average failure stress σ_f and strain ϵ_f values, along with the "pseudo-linear modulus" E_f derived from a tangent fit of the stress-strain curve over the final ~10% strain range (Figure 3-7) are reported in Table 3.4. These parameters, computed from the average strain-to-failure curves of the load-unload cycles from the seven patients, agree well with published values in the literature. The average maximum failure stress for the seven patients was below the levels reported in the literature (Table 3.4).

3.4.2 Biaxial pressurized bulge test

Deflection, area strain, and stress calculations

The membrane deflection profile, derived from the image analysis through MATLAB (see Section 2.3.2), was approximated as a half-ellipse which showed a good fit to the observed deflection (Figure 3-8). The overall bulged membrane area was then computed using axial symmetry, and its associated engineering area strain $\frac{\Delta A}{A_0}$ ($\frac{A-A_0}{A_0}$) and "equivalent" one-dimensional stretch λ were derived (Figure 3-8).

[3]The average failure strain is based on the "maximum displacement" as reported by Oyen et al. and defined as the difference between the displacement at failure and that at which "the load clearly deviates from zero" (see [53] for more details). The somewhat arbitrary nature of this definition may account for the 15% discrepancy between the results of the studies.

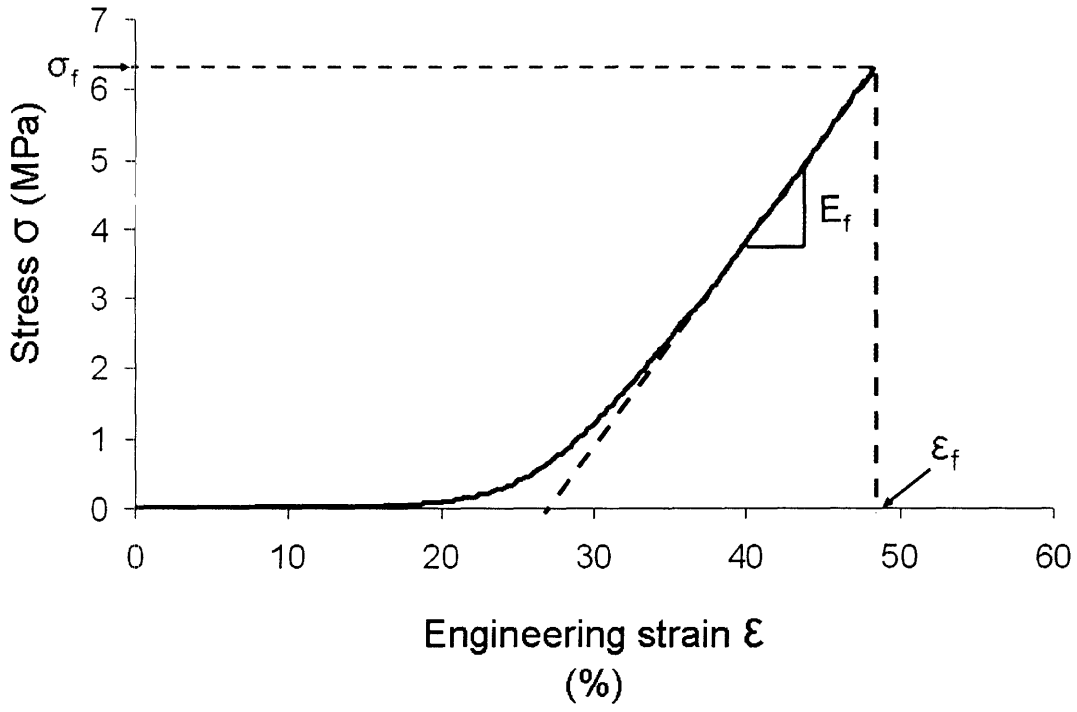

Figure 3-7: Typical stress-strain response of the amnion under uniaxial tension. The engineering strain is defined as $\frac{\Delta L}{L_0}$. Stress calculation is based on a 50 μm amnion thickness. σ_f and ϵ_f refer to the failure stress and strain respectively. E_f corresponds to the "pseudo-linear modulus".

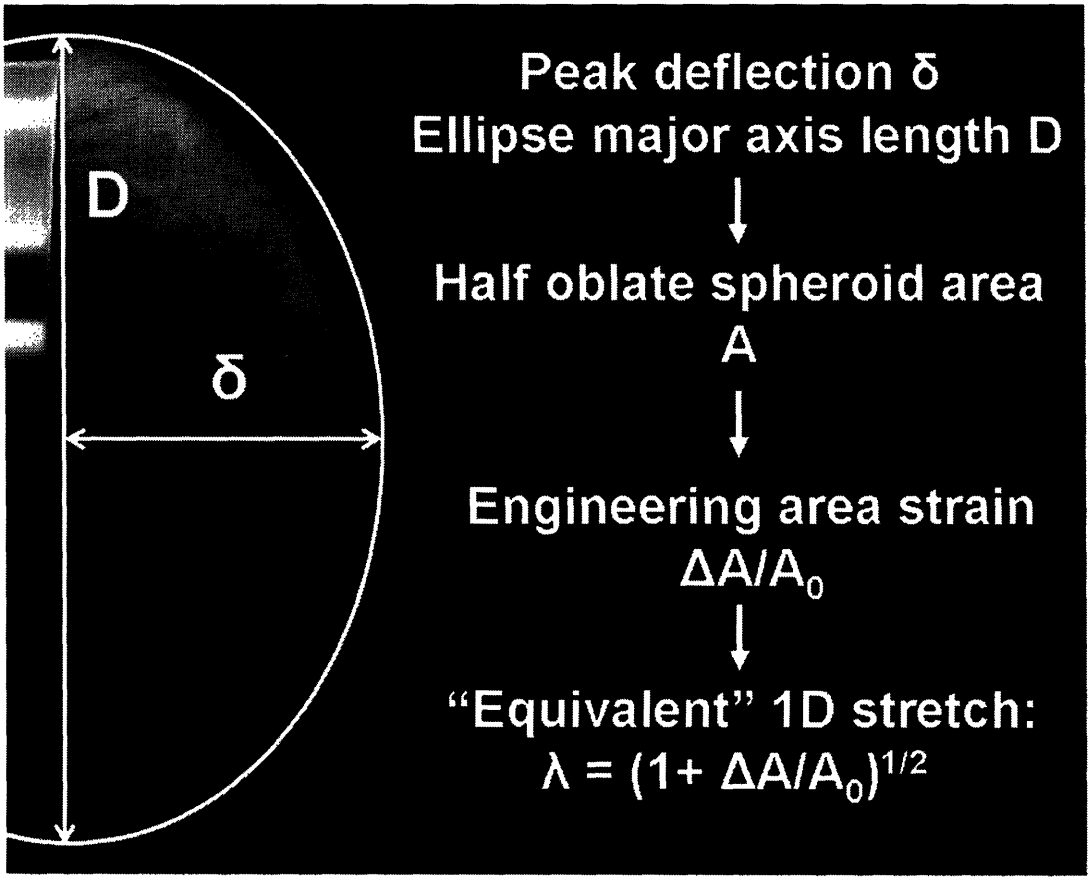

Figure 3-8: Area strain and stretch calculation from membrane deflection profile.

The stress σ was assessed using the thin spherical shell approximation[4]:

$$\sigma = p\frac{r}{2t} \tag{3.2}$$

where p, r and t refer to the applied pressure, the O-ring radius[5] and the membrane thickness respectively.

Results

The results obtained from the seven specimens tested can be seen in Figures 3-9 and 3-10. The average pressure at failure was found to be 10.4 kPa ($\pm$4), value consistent with the previously published estimate [59] of 9.1 kPa ($\pm$4.7)[6]. The engineering area strain at failure was 37.3% ($\pm$6.2). Creep biaxially was found negligible, except during the initial loading step[7] (see Figures 3-9 and 3-11). The creep time constants associated with the initial loading step and calculated from one representative patient were: $t_1 = 28.4\ s$, $t_2 = 274.3\ s$ (Figure 3-11).

3.5 Critical measurement: membrane strain *in vivo*

Given the substantial nonlinearity of the tissue response [63], an accurate assessment of the strain level *in vivo* is critical for an acute mechanical model. Limited estimates of the area strain *in vivo* can be found in the literature: the few measurements performed were based on direct physical uterus inspection [64] or ultrasonography [65]. The average *in vivo* area strain level[8] was found to be 70-100% at term – estimates that are quite large, compared

[4]The membrane thickness was considered negligible compared to the O-ring radius.

[5]A more rigorous r value would be the mean radius of curvature of the deflection profile observed for each step. The use of the O-ring radius instead yields stress values that are underestimates of the real values. This is especially true for the first four steps.

[6]The tests performed by J.P. Lavery et al were based on a 7.62 cm diameter O-ring opening. Their average pressure was therefore rescaled to the new geometry, using Equation 3.1 (ie multiplying by the 7.62/5.4 ratio between the two O-ring's diameters).

[7]The peak displacements resulting from creep were less than 0.4mm, and could not be effectively tracked by the camera whose resolution was of the order of 0.1mm (see Section 2.3.2).

[8]The engineering area strain (%) is defined as $\frac{A_{in\_vivo} - A_{in\_vitro}}{A_{in\_vitro}} \times 100$ where A refers to the membrane area.

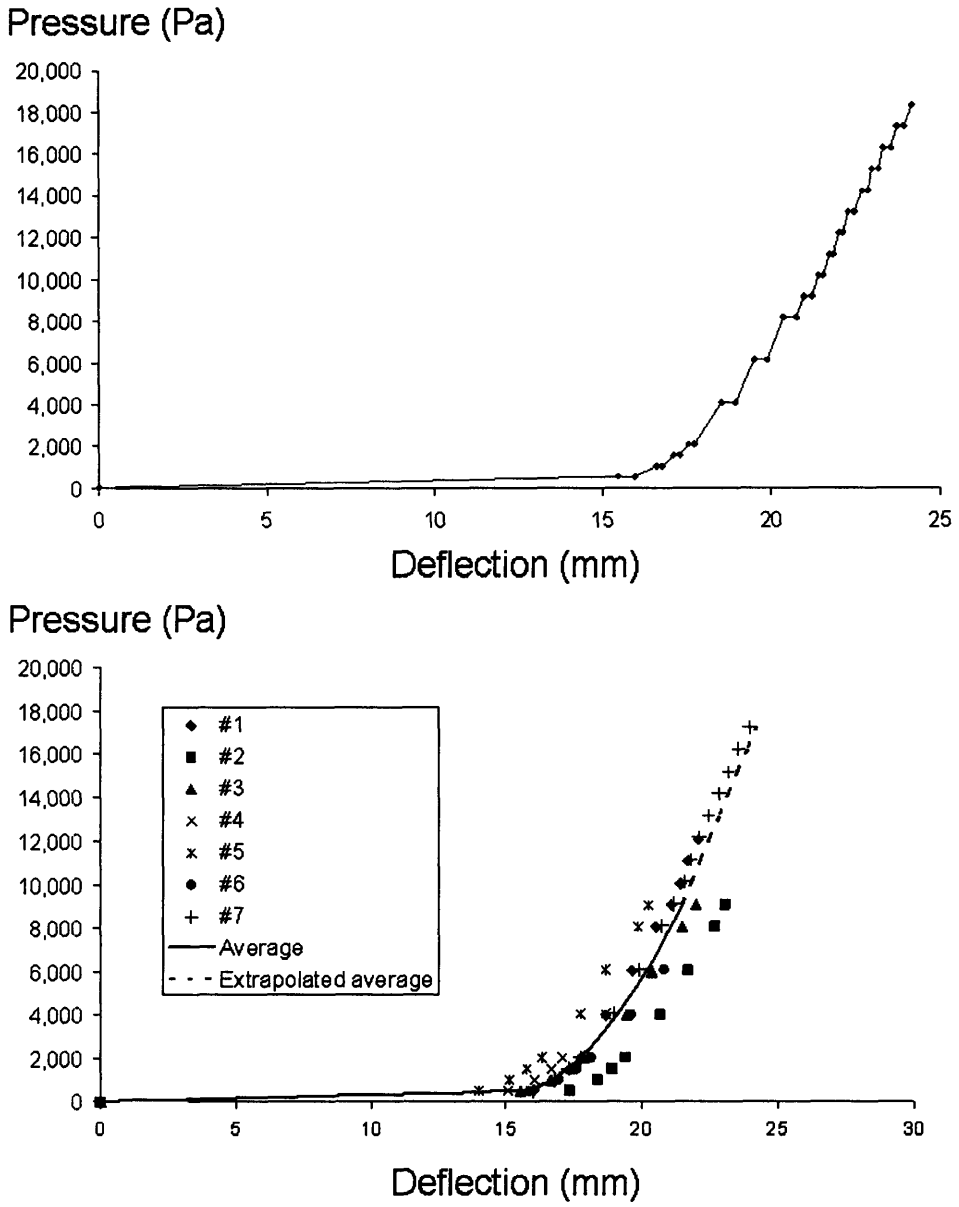

Figure 3-9: Upper graph: applied pressure as a function of time for one representative patient. The instantaneous and final deflections are shown for each 10 minute step. Lower graph: applied pressure as a function of the final deflection (after 10min pressure hold for each step) from the seven CA specimens.

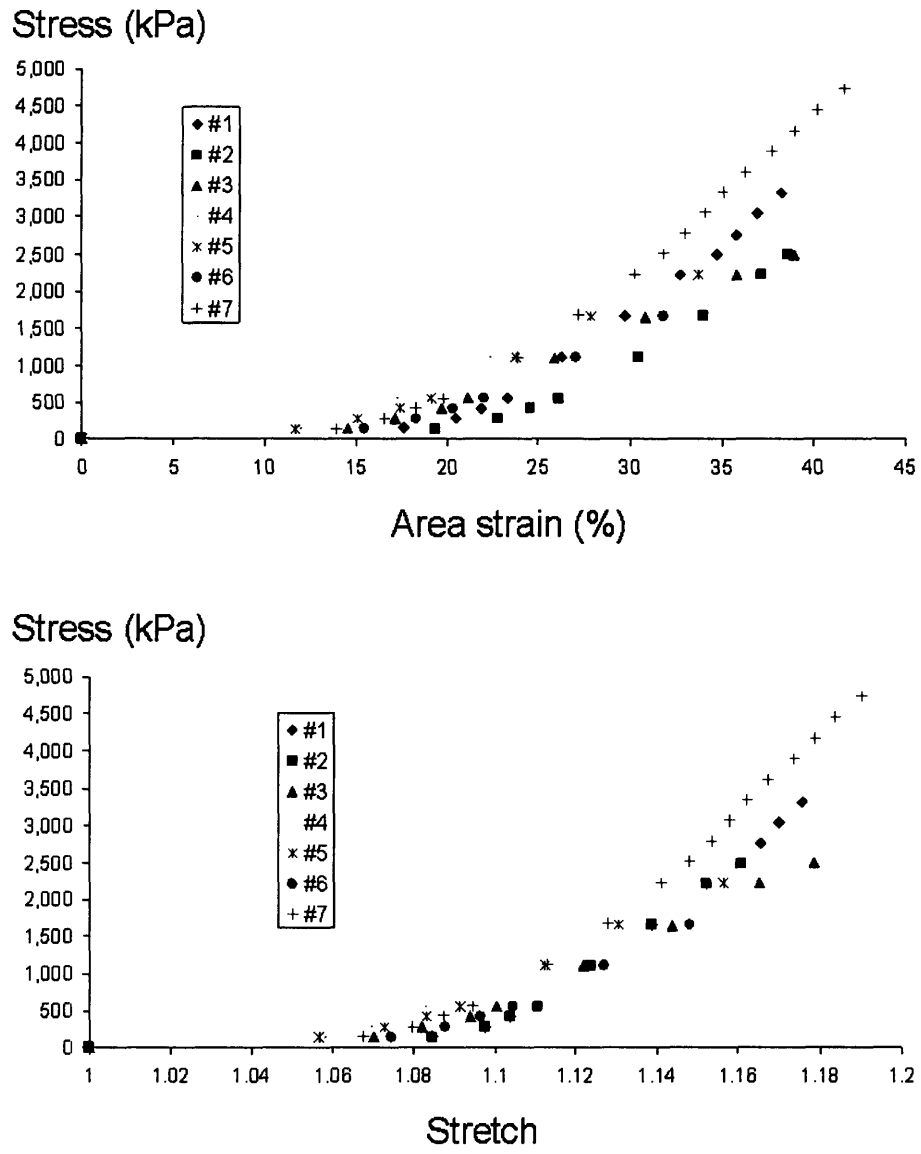

Figure 3-10: Stress - area strain, and stress - equivalent 1D stretch responses from the seven CA specimens tested. Stress calculation is based on a 50 μm thickness.

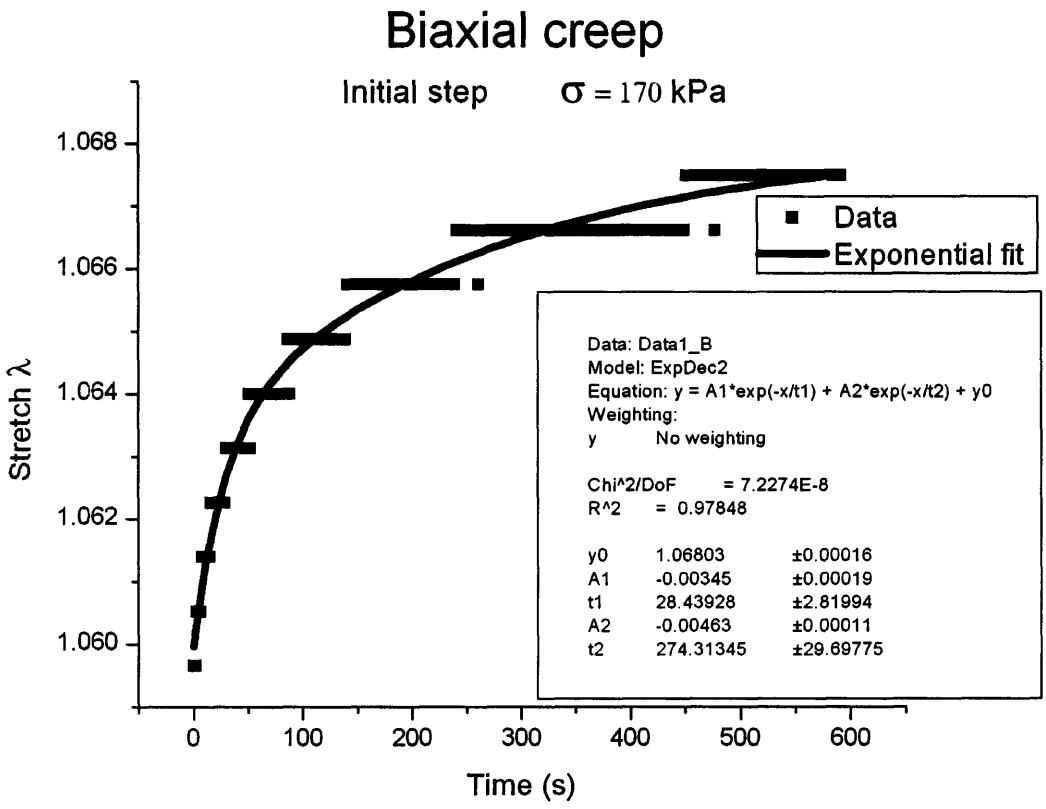

Figure 3-11: Biaxial creep response occurring during the initial 10 minute pressure hold. From one representative specimen.

to our own first *in vitro* assessments of the membrane area strain at failure (see Section 3.4.2 and Figure 3-10). In an effort to obtain more accurate *in vivo* strain assessments, new measurements were performed, using two different techniques: membrane marking and Magnetic Resonance Imaging (MRI).

3.5.1 Membrane marking

A flexible non-deformable template[9] was inserted through an incision made during cesarean section. The template had two half circle slots specifically designed to allow for quick membrane marking with a sterile pen[10]. Once the marking had been performed, following gentle template application on the membrane, and after surgery had been completed, the area of the marked region was measured on the expelled unstretched membrane and compared to that of the initial template. The corresponding area strain level (%) was then derived as:

$$\frac{A_{template} - A_{marked\_region\_in\_vitro}}{A_{marked\_region\_in\_vitro}} \times 100 \tag{3.3}$$

where $A_{template}$ refers to the template area delimited by the two half circles which equals that of the marked membrane region *in vivo*. Although the technique was significantly improved after two to three tries, it has failed to provide reliable results until recently[11].

3.5.2 Magnetic Resonance Imaging (MRI)

In vivo measurements through MRI, however, showed some initial promising results. The procedure was successfully carried out on one patient. MRI imaging was performed at 19 weeks of gestation and the patient delivered one week later. Intrauterine surface area

[9]Much effort was devoted to the designing of the template. The latter had to conform locally to the membrane curvature without undergoing in-plane deformation. As a consequence, the template material had to meet a reasonable "compromise" between relatively high stiffness in plane tension and relatively low stiffness in bending. The final template designed was an approximate 55 × 25 × 1 mm^3 transparent fluorocarbon-based polymer plate pierced with two 14 mm outer diameter 2 mm wide half circle slots.

[10]The time allowed for the procedure could not exceed a few seconds and the surgeon had to ensure that marking was performed away from the presumed rupture point before the membrane bulged out.

[11]The "technical" problems related to the template insertion and its appropriate positioning on membrane surface was overcome, but sterile ink marking tended to either fade away with the amniotic fluid or to extend into larger spilled spots, thereby making any reliable measurement virtually impossible.

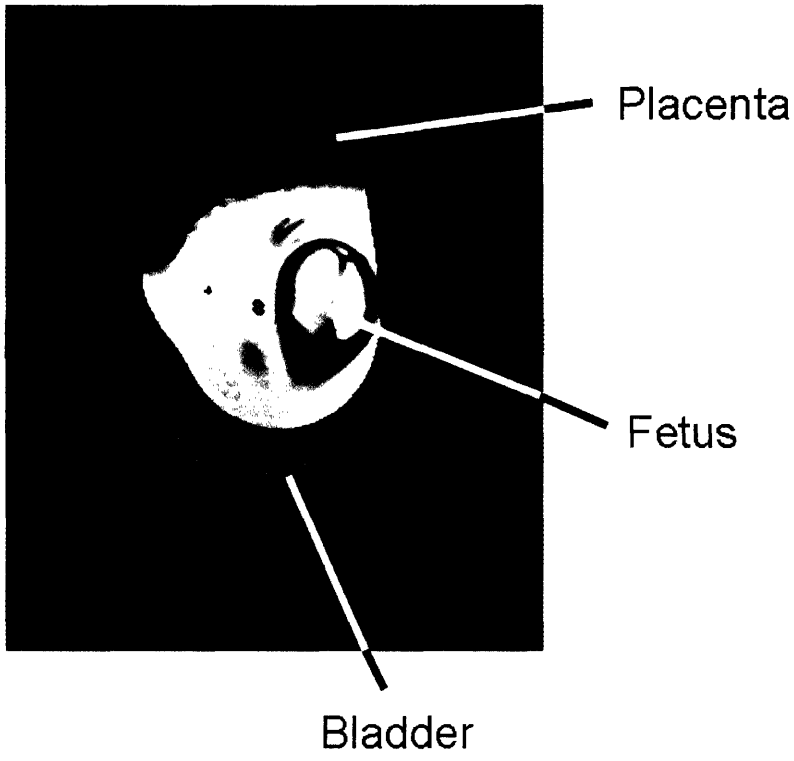

Figure 3-12: MRI image of the uterine cavity. The fetal membrane contour taken into account in the cavity volume reconstruction is marked in red.

	In vitro	In vivo
Placental disc diameter (cm)	10.2 ±0.4 (N=4)	10.5 ±0.4 (N=4)
Chorioamnion surface area (cm^2)	172.6 ±6.5 (N=4)	194.4 ±5.5 (N=2)
Chorioamnion area strain (%)	12.6 (4.8-26.8)	

Table 3.5: Summary of the first in vivo and in vitro area strain measurements.

measurement was achieved in vivo from two independent sets of 14 longitudinal uterus images (Figure 3-12). The volume of the cavity was reconstructed and its corresponding area calculated (including that of the placental disc), using commercial software Analyze 6.0 (AnalyzeDirect, Lenexa KS). The expelled membrane was then carefully cut from the placental edge and laid flat (without stretching and without wrinkles) over a marked grid cutting mat. The *in vitro* surface area of the unstretched membrane and of the placental disc was obtained with a 1 square inch accuracy. In an effort to check the reliability of the technique, the placental disc surface areas measured *in vivo* and *in vitro* were compared and a good match was found (see Table 3.5). The final membrane area strain *in vivo* (ignoring the placental disc) was found to be about 13%. Results are summarized in Table 3.5.

Chapter 4

Modeling and comparison of the model predictions with the experimental results

Continuum [66,67] and molecularly based [68–71] descriptions of biomembrane deformation have been the subject of numerous studies. The continuum model proposed in this study relies on the previous modeling work developed by Febvay [74] on the cervical stroma, with a characteristic planar network structure based on Qi et al [75] membrane modeling suggestions. The chorioamnion is "idealized" as a continuum membrane, whose in-plane response is dominated by the network of collagen fibers (see electron micrograph image in Figure 4-1), where the imposed stretch and the stress state lie in the plane of the membrane. The main constitutive equations are first detailed. The numerical results are then reviewed and compared to those obtained from mechanical testing.

4.1 Collagen planar network

As seen in the first chapter, the collagen fibers are thought to dominate the mechanical response of the fetal tissue. The assembly of collagen fibers via chemical cross-links gives it a network-like structure similar to that of a polymer network. A model derived from mechanics theories developed in rubber elasticity [76,77] is used to represent the collagen network of the

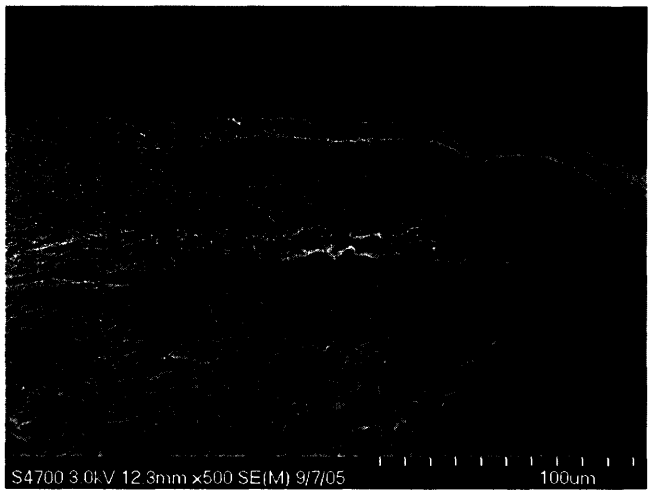

Figure 4-1: Scanning electron micrograph revealing the multi-sheet collagen structure of the compact and fibroblast layers beneath a thin epithelial cell layer. The amnion is folded upon itself. Micrograph picture of the amnion taken by Dr. Steven Calvin at University of Minnesota.

chorioamnion. This type of models for hyperelastic materials rely on two fundamental steps. First, a force-stretch relationship must be defined for the individual chains of the network; second, a simple representative unit structure must be defined to account for the geometry of the network, in order to enable the link between macroscopic deformation variables and the deformation of the individual chains. The following sections describe in detail the structures adopted for these elements in the case of the chorioamnionic collagen.

4.1.1 Individual chain force-stretch relationship

A collagen fibril is "idealized" as a chain with a certain number of rigid links that can rotate with respect to each other. An increase in length would result in a reduction of the number of possible configurations for the building links of the fibril, and thus lead to a decrease in entropy. This decrease corresponds to an increase of the entropic portion ($-Ts$) of the free energy, responsible for the observed stress (T is the absolute temperature and s the entropy of the chain). This model leads to simple force-stretch relationships for individual fibrils, based on the number of links per chain, and the statistical model used to represent

the possible configurations of a chain at a given length.

Several statistical models have been used to represent chain configurations. The approach adopted by Kuhn and Grühn in 1942 [77] uses Langevin chain statistics, which yields the following expression for the force f developed in a chain in response to a given stretch λ:

$$f = \frac{k_B T}{b} \mathcal{L}^{-1}\left(\frac{r}{nb}\right) = \frac{k_B T}{b} \mathcal{L}^{-1}\left(\frac{\lambda}{\sqrt{n}}\right), \tag{4.1}$$

where k_B is Boltzmann's constant, T is the temperature, r is the length of the chain, b is the length of a rigid link, n is the number of such links in a chain, and $\mathcal{L}^{-1}$ is the inverse Langevin function defined by

$$\beta = \mathcal{L}^{-1}\left(\frac{r}{nb}\right), \tag{4.2}$$

$$\frac{r}{nb} = \mathcal{L}(\beta) = \coth\beta - \frac{1}{\beta}. \tag{4.3}$$

The fully extended length of a chain is nb, and the average initial length of a chain is given by $\sqrt{n}b = l_0$. The stretch λ is consequently given by $\lambda = \frac{r}{l_0} = \frac{r}{\sqrt{n}b}$. Finally, the limiting or locking stretch corresponds to $\lambda_L = \sqrt{n}$.

4.1.2 Representative network structure

The second step in model development consists in defining an average representative structure for the network, in order to establish a link between the individual chains response and the global deformation. The most common approach to this problem is to assume the network to be represented by a unit cell that deforms with the principal stretches of the deformation. The representative chain configuration we assume in the unit cell is based on the model proposed by Qi et al [75] for protein planar networks, defined by a square unit cell with 4 individual chains connected at the center (see Figure 4-2).

The cell deforms with the principal stretches. The symmetry of the cell is such that the junction point remains at the center during the whole deformation, and all the chains

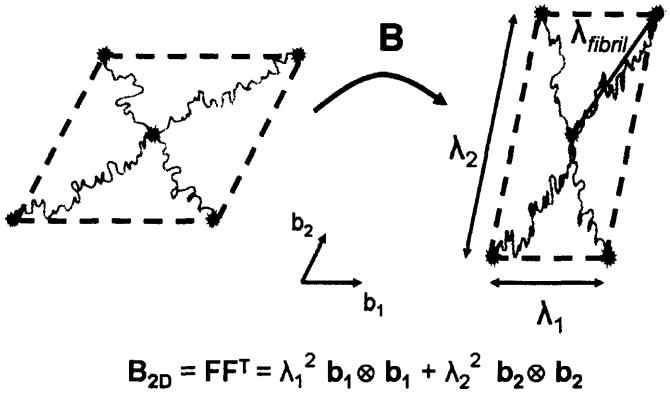

Figure 4-2: The 4-fibril unit cell. The cell is taken to deform along the principal directions of the planar left Cauchy-Green tensor.

experience the same level of stretch, given by

$$\lambda_{\text{fibril}} = \sqrt{\frac{\lambda_1^2 + \lambda_2^2}{2}}, \tag{4.4}$$

where λ_1, and λ_2 are the principal stretches. In addition to having the same stretch, the chains rotate towards the directions of highest stretch, as can be seen in Figure 4-2. This captures the effect of network orientation produced by the applied deformation.

4.1.3 Stress-Strain Constitutive Behavior

The four-fibril network, together with the force-stretch relationship used to represent the behavior of a collagen fibril, can be integrated to derive a full 2-dimensional stress-strain relationship for the collagen network. This can be done by calculating the strain energy density associated with this representative structure. The hyperelastic strain energy density of the whole network, W_{Col}^{2D}, can be calculated as the strain energy of a single collagen fibril

w_{fibril}, multiplied by the areal density of fibrils in the network N:

$$W_{Col}^{2D} = N w_{\text{fibril}}, \tag{4.5}$$

with the strain energy of an individual fibril given by

$$w_{\text{fibril}} = \int f_{\text{fibril}} dl_{\text{fibril}} = \int f_{\text{fibril}} l_0 d\lambda_{\text{fibril}}, \tag{4.6}$$

where the fibril stretch λ_{fibril} is related to the principal stretches λ_i by equation (4.4), and the corresponding fibril force f_{fibril} is defined by equation (4.1). Integration yields the following expression for the strain energy density:

$$W_{Col}^{2D} = N k_B T \lambda_L \left[\beta_{\text{fibril}} \lambda_{\text{fibril}} + \lambda_L \ln \left(\frac{\beta_{\text{fibril}}}{\sinh \beta_{\text{fibril}}} \right) + \frac{\beta_0}{2} \ln \frac{1}{J} \right], \tag{4.7}$$

where

$$\beta_{\text{fibril}} = \mathcal{L}^{-1} \left(\frac{\lambda_{\text{fibril}}}{\sqrt{n}} \right) = \mathcal{L}^{-1} \left(\frac{\lambda_{\text{fibril}}}{\lambda_L} \right) \quad ; \quad \beta_0 = \mathcal{L}^{-1} \left(\frac{1}{\lambda_L} \right)$$

and J is the areal Jacobian[1] defined by $J = \lambda_1 \lambda_2$. The third term of equation 4.7 ($\beta_0 \ln \frac{1}{J}$) has been introduced to account for the small contribution of internal energy, which prevents entropic collapse of the network, and ensures zero stress in the absence of deformation.

The associated Cauchy membrane stress $\mathbf{T}_{\mathrm{C}}^{2D}$ is then obtained by differentiation of the strain energy density with respect to the invariants of the planar left Cauchy-Green tensor $\mathbf{B}_{2D}$:

$$\mathbf{T}_{\mathrm{C}}^{2D} = \mathbf{T}_{\mathrm{C}}.h = \frac{2}{J} \frac{\partial W_{Col}^{2D}}{\partial I_1} \mathbf{B}_{2D} + \frac{\partial W_{Col}^{2D}}{\partial J} \mathbf{I}_{2D} \tag{4.8}$$

$$\mathbf{B}_{2D} = \mathbf{F}\mathbf{F}^{\mathbf{T}} \qquad I_1 = tr\mathbf{B}_{2D} = \lambda_1^2 + \lambda_2^2 \qquad J = det\mathbf{F} = \sqrt{det\mathbf{B}_{2D}} = \lambda_1 \lambda_2 \tag{4.9}$$

$$h: \text{ membrane initial thickness} \qquad \mathbf{T}_{\mathrm{C}}: \text{ Cauchy stress} \tag{4.10}$$

[1] J corresponds experimentally to λ^2, defined in Section 3.4.2, where λ refers to the "equivalent" one-dimensional stretch.

By differentiation, the following expression is obtained for the stress $\mathrm{T}_{\mathrm{C}}^{2D}$:

$$\mathrm{T}_{\mathrm{C}}^{2D} = \frac{Nk_BT\lambda_L}{2}\frac{1}{J}\left[\frac{\beta_{\text{fibril}}}{\lambda_{\text{fibril}}}\mathbf{B}_{2D}-\beta_0\mathbf{I}_{2D}\right] \tag{4.11}$$

Finally, an areal corrective term can be added to the stress to account for additional energetic contributions to the strain energy density:

$$\mathrm{T}_{\mathrm{C}}^{2D} = \frac{Nk_BT\lambda_L}{2}\frac{1}{J}\left[\frac{\beta_{\text{fibril}}}{\lambda_{\text{fibril}}}\mathbf{B}_{2D}-\beta_0\mathbf{I}_{2D}\right] + K_{\mathrm{A}}\left(J-1\right)\mathbf{I}_{2D} \tag{4.12}$$

The membrane response is then defined in terms of the three following material properties:

- the quantity $\frac{Nk_BT\lambda_L}{2}$, equivalent to an "initial shear modulus",
- the limiting stretch $\lambda_L = \sqrt{n}$ for the collagen fibrils,
- and the additional areal expansion modulus K_{A}.

4.1.4 Stretch criterion

As shown in Figure 3-7, the tissue behavior in tension is characterized by an initial compliant response followed by a substantial increase in stiffness. These response features are initially well captured by the Langevin function defining the force-stretch relationship of individual collagen fibrils. The latter function, however, diverging as the stretch appoaches λ_L, fails to describe the characteristic linear tissue behavior at large strains preceding failure. To capture this feature of the response, a critical extension λ_{linear} was defined for the model, beyond which the Langevin function used to describe the collagen network response was replaced by the simple affine function derived from the tangent fit detailed in Section 3.4.1.

4.2 Time-dependent response

We propose that the viscous response of the chorioamnionic tissue is driven by the in-plane shear stresses. The absence of creep behavior observed in the bulge experiment substantiates this hypothesis. The resulting viscous deformation is therefore constrained to be isochoric.

The deformation gradient $\mathbf{F}$ can be expressed in terms of its isochoric component $\mathbf{F}_{\text{iso}}$ as:

$$\mathbf{F} = \sqrt{J}\mathbf{F}_{\text{iso}} \tag{4.13}$$

where J is the areal Jacobian defined earlier.

The velocity gradient corresponding to the imposed plastic deformation is

$$\mathbf{L} = \dot{\mathbf{F}}_{\text{iso}}\mathbf{F}_{\text{iso}}^{-1} = \overset{\bullet}{(\mathbf{F}_{\text{iso}}^{e}\mathbf{F}_{\text{iso}}^{f})}(\mathbf{F}_{\text{iso}}^{e}\mathbf{F}_{\text{iso}}^{f})^{-1} = (\dot{\mathbf{F}}_{\text{iso}}^{e}\mathbf{F}_{\text{iso}}^{f} + \mathbf{F}_{\text{iso}}^{e}\dot{\mathbf{F}}_{\text{iso}}^{f})\mathbf{F}_{\text{iso}}^{f\,-1}\mathbf{F}_{\text{iso}}^{e\,-1}, \tag{4.14}$$

where the isochoric deformation gradient has been decomposed into its elastic ($\mathbf{F}_{\text{iso}}^{e}$) and flow or viscous part ($\mathbf{F}_{\text{iso}}^{f}$). The contributions of the elastic and flow parts of the deformation can then be separated as

$$\mathbf{L} = \underbrace{\dot{\mathbf{F}}_{\text{iso}}^{e}\mathbf{F}_{\text{iso}}^{e\,-1}}_{\mathbf{L}_{\text{iso}}^{e}} + \underbrace{\mathbf{F}_{\text{iso}}^{e}\dot{\mathbf{F}}_{\text{iso}}^{f}\mathbf{F}_{\text{iso}}^{f\,-1}\mathbf{F}_{\text{iso}}^{e\,-1}}_{\tilde{\mathbf{L}}_{\text{iso}}^{f}} = \mathbf{L}_{\text{iso}}^{e} + \tilde{\mathbf{L}}_{\text{iso}}^{f}. \tag{4.15}$$

The flow contribution to the velocity gradient is separated in its skew and symmetric parts, which need to be constitutively prescribed:

$$\tilde{\mathbf{L}}_{\text{iso}}^{f} = \tilde{\mathbf{D}}_{\text{iso}}^{f} + \tilde{\mathbf{W}}_{\text{iso}}^{f}. \tag{4.16}$$

The plastic spin can be prescribed to be zero to ensure uniqueness of the decomposition as proposed by Boyce et al in the case of a constitutive model for polyethylene terephtalate [78]. The plastic rate of stretching is prescribed as being proportional to the deviatoric stress $\mathbf{T}'$:

$$\begin{cases} \tilde{\mathbf{W}}_{\text{iso}}^{f} &= 0 \text{ (no spin)} \\ \tilde{\mathbf{D}}_{\text{iso}}^{f} &= \dot{\gamma}^{f}\mathbf{N} \end{cases} \tag{4.17}$$

where $\mathbf{N}$ is the tensorial direction of $\mathbf{T}'$, given by

$$\mathbf{N} = \frac{1}{\sqrt{2}\tau}\mathbf{T}' \qquad \tau = \sqrt{\frac{1}{2}\mathbf{T}' : \mathbf{T}'}, \tag{4.18}$$

and $\mathbf{T}'$ is the deviatoric Cauchy membrane stress

$$\mathbf{T}' = \mathbf{T}^{2D} - \frac{1}{3}(tr\mathbf{T}^{2D})\mathbf{I}. \tag{4.19}$$

The flow strain rate coefficient $\dot{\gamma}^f$ needs to be constitutively prescribed for the response of the viscous element of the model to be fully characterized. The underlying physical mechanisms involved in the viscous flow are frictional in nature, coming from interactions between adjacent collagen fibers as well as from friction forces between GAG chains and collagen fibrils or interstitial water. Given the non linear viscous tissue response derived from a preliminary second order exponential fit of the experimental stress relaxation and creep responses (see Figures 3-5 and 3-6), we adopted a power law relationship between the deviatoric stress $\mathbf{T}'$ and the rate of stretching associated with the flow:

$$\dot{\gamma}^f = \dot{\gamma}_0(\frac{\tau}{s})^m, \tag{4.20}$$

where $\dot{\gamma}_0$, s and m are material properties to be fitted to the data.

The stress $\mathbf{T}^{2D}$ in the viscoelastic material is obtained from the elastic component of the deformation gradient following expression 4.12, where:

$$\begin{aligned} \beta^{\mathrm{e}}_{\mathrm{fibril}} &= \mathcal{L}^{-1}\left(\frac{\lambda^{\mathrm{e}}_{\mathrm{fibril}}}{\lambda_L}\right) \quad ; \quad \lambda^{\mathrm{e}}_{\mathrm{fibril}} = \sqrt{\frac{I^e_1}{2}} \\ I^e_1 &= tr\mathbf{B}^e_{2D} = tr(\mathbf{F}^e\mathbf{F}^{e\mathbf{T}}) = tr(J\mathbf{F}^e_{\mathrm{iso}}\mathbf{F}^{e\mathbf{T}}_{\mathrm{iso}}) \end{aligned} \tag{4.21}$$

4.3 Numerical implementation

4.3.1 Results

The mechanical model was implemented using commercial finite element software (ABAQUS 6.5). The constitutive equations describing the fetal tissue behavior and detailed in the previous sections of this chapter were coded as a user material subroutine UMAT. The model proposed is still at an early stage of development, and its numerical implementation,

as of now, does not include the time-dependent response.

The simulations performed for the biaxial pressurized bulge test were implemented using axisymmetric elements, taking advantage of the problem cylindrical symmetry. The model parameters λ_L, λ_{linear}, K_A and $\frac{Nk_BT\lambda_L}{2}$ detailed in Section 4.1 were fit to the data from one typical patient.

The latest numerical results obtained are presented in Figures 4-3, 4-4, 4-5 and 4-6 for the uniaxial load-unload cycle response and the bulge test response, using one common set of parameters ($\lambda_L = 1.06$, $\lambda_{linear} = 1.055$, $K_A = 10\ Mpa$, $\frac{Nk_BT\lambda_L}{2} = 800\ Pa$). The contribution of the chorion to the global tissue mechanical response was neglected.

4.3.2 Discussion

The model predictions agree well with the uniaxial "elastic" response of the tissue (Figure 4-4). However, the model fails to capture the membrane initial compliant response under biaxial stress. Further work would be needed to fully account for the membrane deformation under both modes of deformation, and to incorporate the time-dependent response of the material.

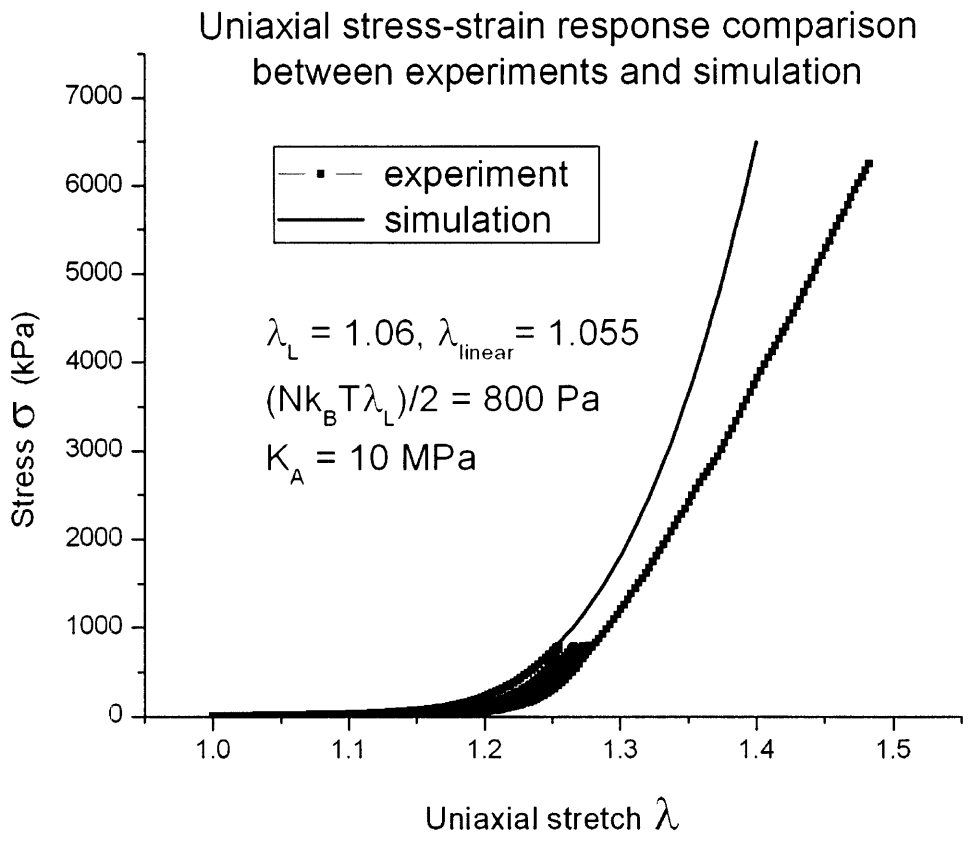

Figure 4-3: Uniaxial load-unload cycles from one typical patient. Results are compared to the hyperelastic strain-to-failure curve from the model.

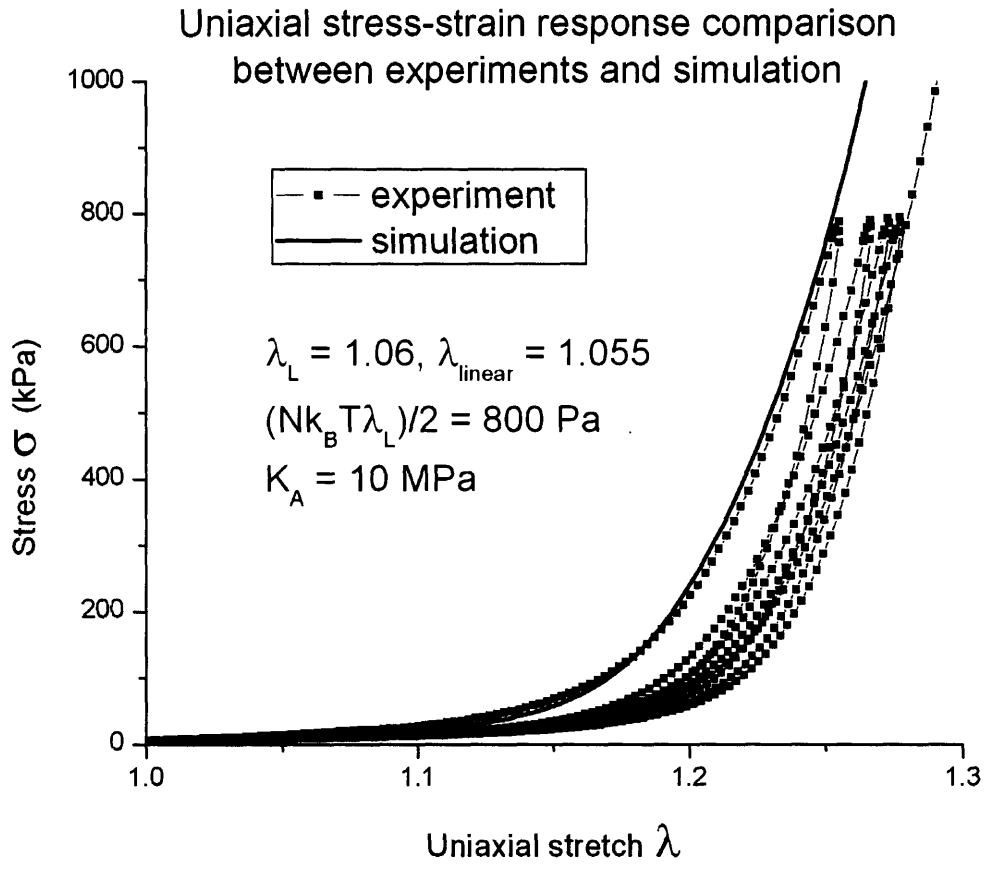

Figure 4-4: Uniaxial load-unload cycles. Average stress-stretch curve from one typical patient compared to the hyperelastic model predictions.

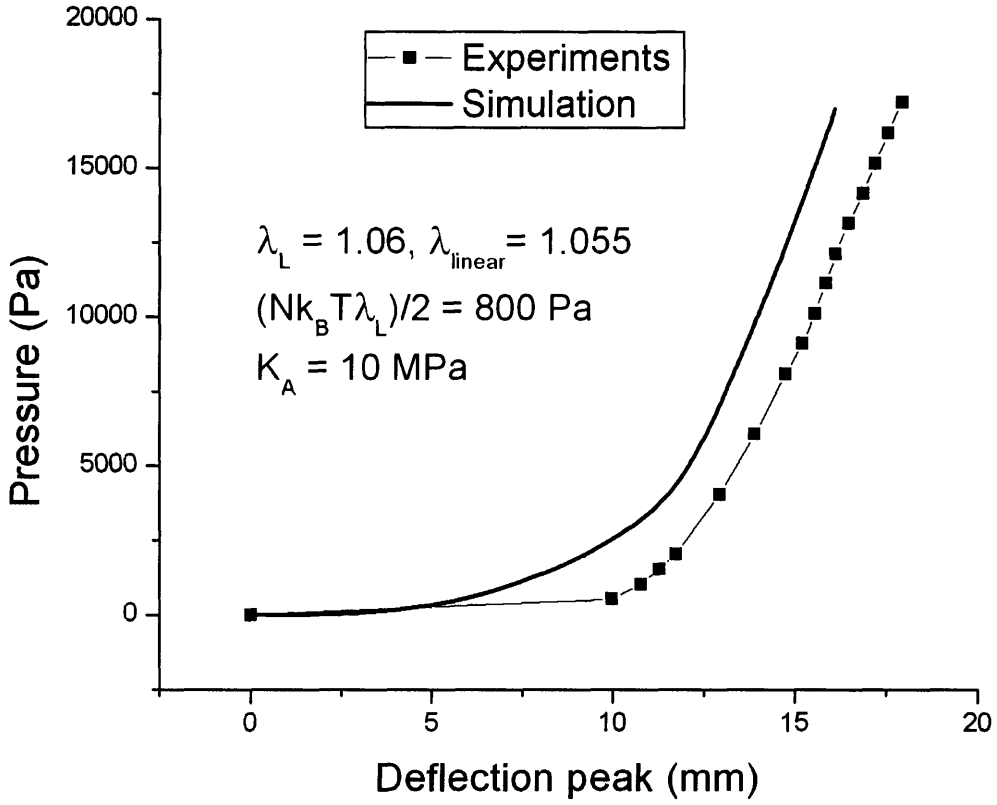

Figure 4-5: Biaxial pressurized bulge test. Applied pressure vs membrane deflection peak curve compared to the hyperelastic model predictions.

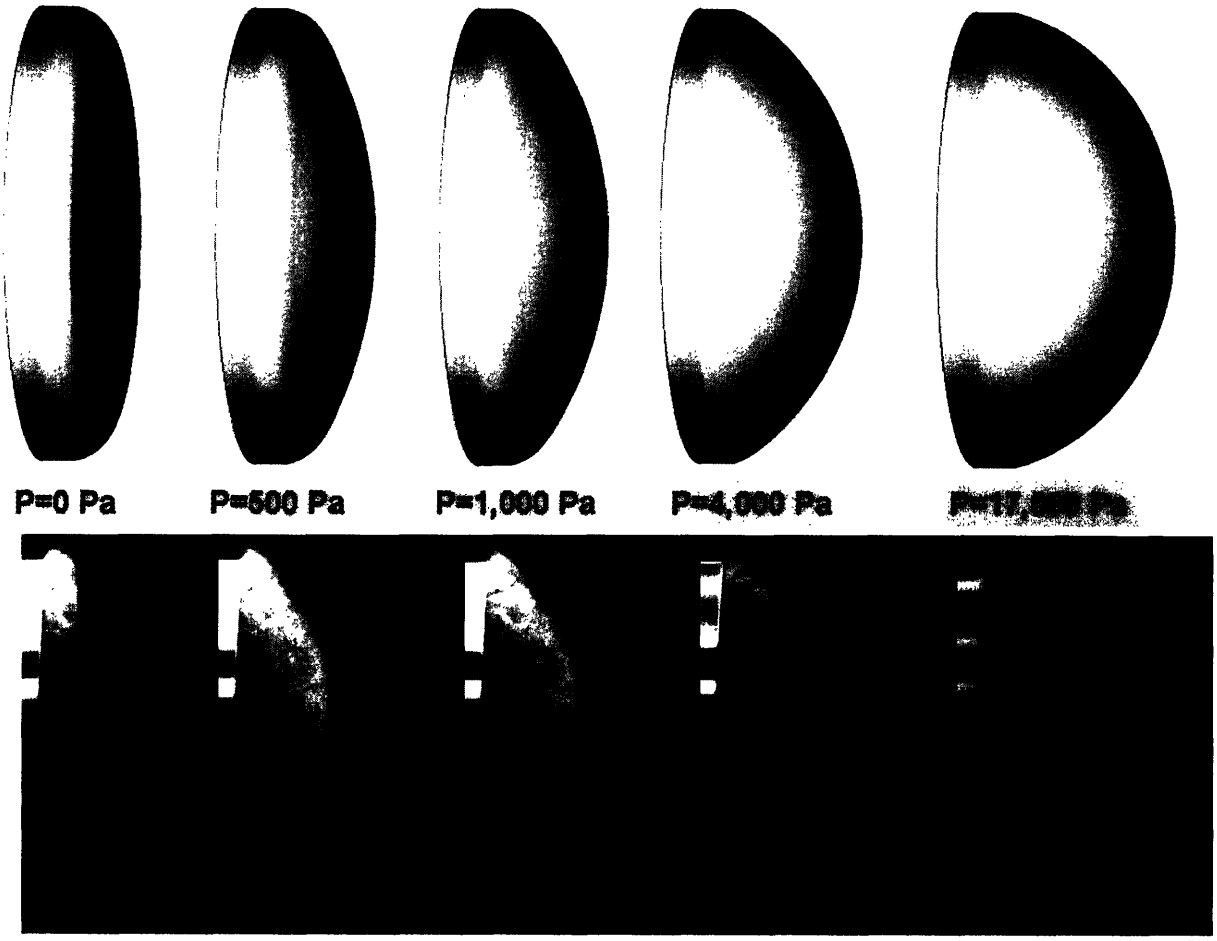

Figure 4-6: Biaxial pressurized bulge test: membrane in vitro response compared to the model's predictions. $\lambda_L = 1.06$, $\lambda_{linear} = 1.055$, $K_A = 10\ Mpa$, $\frac{Nk_BT\lambda_L}{2} = 800\ Pa$.

Chapter 5

Conclusion and recommendations for future work

5.1 Conclusion

This study was aimed at characterizing the chorioamnion mechanical behavior *in vitro*, along with its biochemical properties. To achieve this objective, specific experimental protocols regarding both the handling and the testing of the fetal tissue were devised. The latter concern:

- chorioamnion collection and preparation for testing
- amnion uniaxial testing
- chorioamnion biaxial testing
- chorion and amnion thickness measurement
- chorion and amnion biochemical testing (measurements of hydration level, A/C wet and dry mass ratios, collagen and sulfated glycosaminoglycan contents, collagen extractability).

These protocols were successfully implemented on CA samples from seven patients. The collagen and sulftated glycoasminoglycan contents were measured. The amnion uniaxial

tensile testing results agreed well with those previously published in the literature. They demonstrated a nonlinear viscoelastic response characterized by substantial relaxation and creep.

The biaxial pressurized bulge tests performed on the chorioamnion revealed that:

- tissue failure occurred around 40% area strain
- creep was negligible under equibiaxial stress (compared to the levels observed uniaxially)

In addition to the systematic biomechanical testing procedures developed *in vitro* for the chorioamnion, first reliable area strain measurement techniques were developed *in vivo* through MRI. These promising preliminary strain assessments would need to be developed further in order to obtain statistically relevant results.

A constitutive model relying on the collagen network elastic response and integrating the nonlinear time-dependent response of the amnion was also proposed. The hyperelastic component of the model was numerically implemented. The simulation results agree well with the tissue uniaxial strain-to-failure response but fail to fully capture the initial compliant response observed under biaxial mode.

5.2 Recommendations for future work

Experimentally, the following may be pursued:

1. improvement of membrane thickness measurement
2. development of biaxial cyclic loading at low pressure levels to more accurately capture the tissue viscoelastic behavior in biaxial mode
3. investigation of membrane crack initiation and propagation
4. assessment of the area strain *in vivo*

Numerically, a refined model would be needed, able to capture the initial compliant response of the tissue in biaxial mode and integrating the constitutive equations proposed for the nonlinear viscoelastic response of the tissue.

This should then pave the way for quantitative correlations between tissue microstructure, biochemical properties (such as collagen and proteoglycan contents) and macroscopic mechanical response.

Appendix A

Membrane Clinical variables

1. Number (singleton - twins, monozygotic - twins, dizygotic - triplets+)
2. Gender(s)
3. Gestational age (in completed weeks)
4. Maternal age
5. Race (Hispanic, African American, Non-Hispanic White, Asian etc)
6. Obstetrical history (number of previous pregnancies, type of delivery, etc)
7. Prior preterm delivery (yes/no)
8. Chorioamnionitis
9. Smoking (yes/no)
10. Diabetes (yes/no)
11. Preeclampsia (yes/no)
12. Amniocentesis (yes/no)
13. Cerclage (yes/no)
14. In vitro fertilization (yes/no)

15. Placenta Previa (yes/no)

16. Fetal Fibronectin tested (yes/no)

17. Group B Strep Status (positive/negative)

18. Tocolytics (yes/no)

19. Induction agent (yes/no)

20. Pitocin use (yes/no)

21. $MgSO_4$ (yes/no)

22. Antibiotic use (yes/no)

23. Meconium (yes/no)

24. Cervical dilation (yes/no)

25. Mode of delivery (vaginal, C/section with labor, C/section without labor)

26. Indication for delivery

Appendix B

Mechanical Testing and Thickness Measurement Protocols

B.1 Collecting Chorioamnionic Membrane from the New England Medical Center

B.1.1 Materials

- Plastic specimen container (from hospital)
- Surgical scissors (from hospital)
- Stainless steel tweezers (from hospital)
- Sterile saline solution (from hospital)
- Zip-close clear bag (VWR Catalog #89005-296)

B.1.2 Procedure

1. Collect placenta from operating room after delivery.
2. Cut an approximate 20×20 cm^2 piece of CA, using surgical scissors. Start from placental disc's edge. Handle tissue with care.

3. Rinse specimen in sterile saline.

4. Save an approximate 2×5 cm^2 strip for histology and place the remaining piece in sterile fluid container with saline solution.

5. Place fluid container on ice in zip-close bag and transport specimen to laboratory for immediate testing.

B.2 Pressurized Bulge Test with CA Specimen

B.2.1 Equipment and materials

- Camera (QImaging Retiga 1300 CCD camera)
- Computer with Vic-Snap software (version 3.0D, Correlated Solutions, Inc)
- 1 m rigid aluminum rod
- 30×20 cm^2 aluminum square
- Fluid box and accessories (see Figure B-1 and Engineering drawings in Appendix D)
- Thermometer
- 45 mm Rotary cutter (Fiskars Catalog #95217097)
- 45 mm Rotary straight blade (Fiskars Catalog #95287097)
- 12in.×18in. Self-healing cutting mat (Fiskars Catalog #86117097)
- 5 psi range pressure transducer (Sensotec FPG1AT)
- Pressure signal indicator (Sensotec, Model GM-A)
- Phosphate Buffered Saline (PBS - 10× VWR Catalog #EM-6508)
- Timer

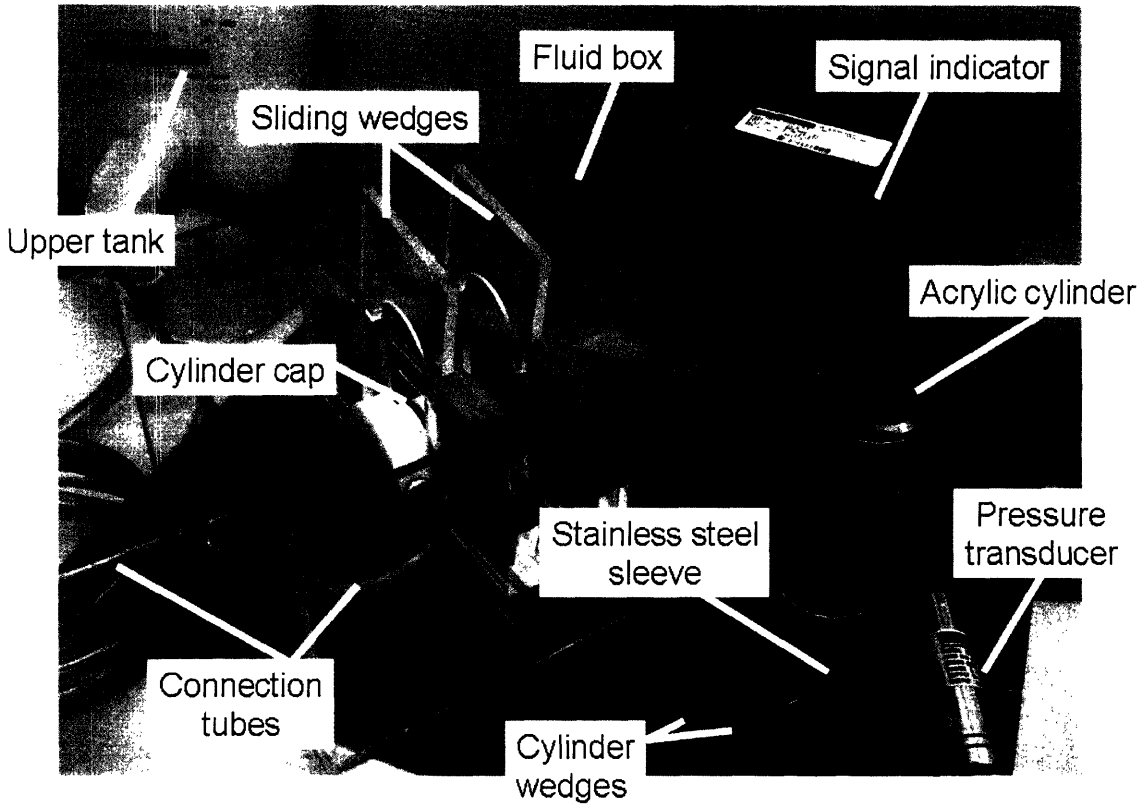

Figure B-1: Materials for biaxial testing.

B.2.2 Procedure

Biaxial apparatus preparation guidelines

1. Connect camera to laptop and open a new Vic-Snap software file.
2. Adjust fluid box edges perpendicular to camera direction, using rigid aluminum rod and square. Make sure that camera is focused on testing area.
3. Fill fluid box and upper tank with saline (upper tank is closed at this point). Make sure that there is no significant height difference between the two saline baths' levels.
4. Open upper tank and wait for about 15min to allow pressure to equilibrate between the saline baths in fluid box and upper tank.
5. Place thermometer into bath, and note temperature.

CA membrane cutting and loading

1. Rinse membrane thoroughly in saline until blood color disappears.
2. Humidify cutting mat with saline and lay membrane flat over mat.
3. Cut an approximate 9×9 cm^2 CA piece from specimen using rotary cutter (Figure B-2, Step 1).
4. Mount specimen carefully on cylinder edge, chorion outwards (Figure B-2, Step 2). Make sure that specimen is neither slack nor stretched.
5. Adjust stainless sleeve on upper part of cylinder and tighten specimen gently using screwdriver (Figure B-2, Step 3). Make sure sleeve is adjusted at the very edge of cylinder.
6. Adjust the specimen onto fluid box supporting framework, using cylinder grooves to "anchor" it (Figure B-2, Step 4). Cylinder extension for pressure transducer must be oriented upwards.

7. Seal bottom part of cylinder, using teflon cap (connected to upper tank) and stainless steel wedges (Figure B-2, Step 4).

8. Screw pressure transducer into cylinder extension.

9. Place sliding wedges on top of cylinder to completely stabilize the structure.

Testing

1. Note down initial pressure level measured by transducer.

2. Start timer and camera recording simultaneously. Lift tank **immediately** along sliding pole by the desired height, using reference levels marked on pole (it should not last more than 3-4 seconds).

3. Note the time needed for pressure to equilibrate (approximately 5-20 seconds) along with the pressure value at equilibrium.

4. Let test run for 10 minutes.

5. Repeat steps 2-4 for each new pressure increment until membrane failure occurs.

B.3 Uniaxial Tensile Test with Amnion Specimen

B.3.1 Equipment and Materials

- Uniaxial testing machine (Zwick Z2.5/TSIS, Ulm, Germany)
- Camera (QImaging Retiga 1300 CCD camera)
- Computer with Vic-Snap software (version 3.0D, Correlated Solutions, Inc)
- Thermometer
- 45 mm Rotary cutter (Fiskars Catalog #95217097)
- 45 mm Rotary straight blade (Fiskars Catalog #95287097)

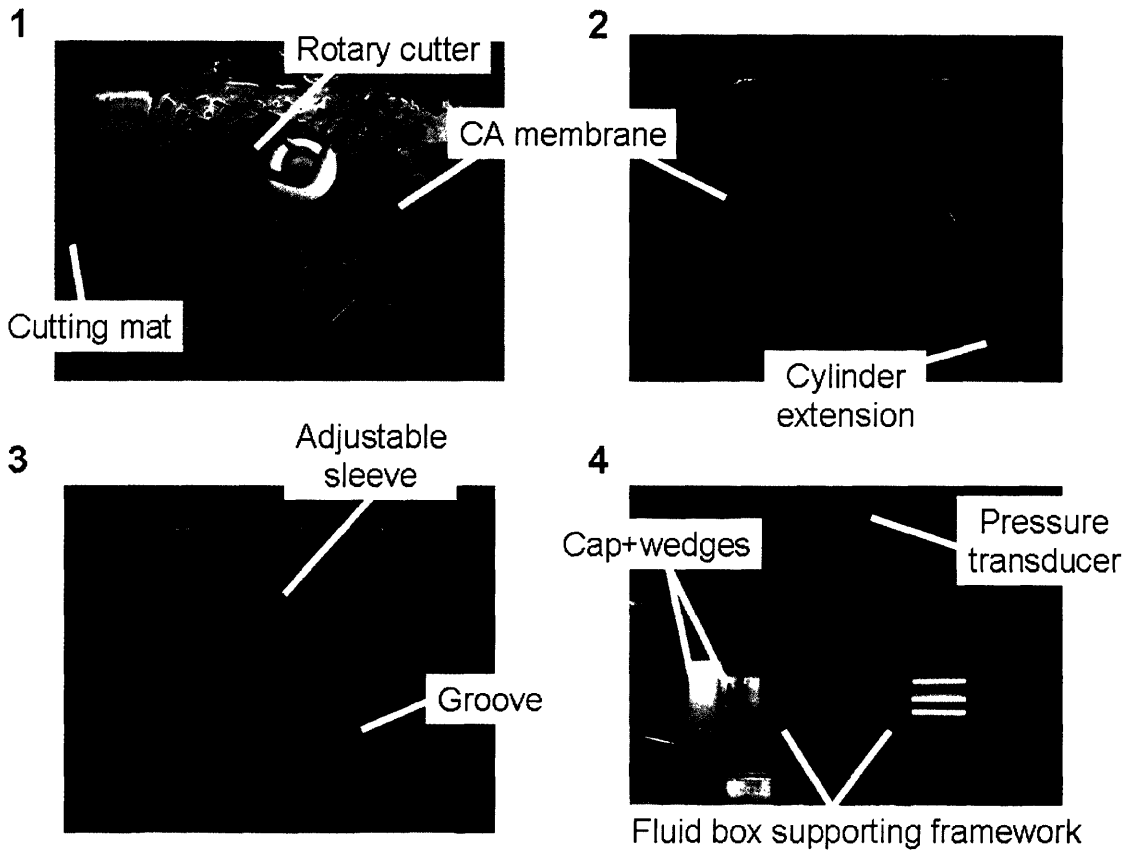

Figure B-2: Pressurized bulge test: main steps.

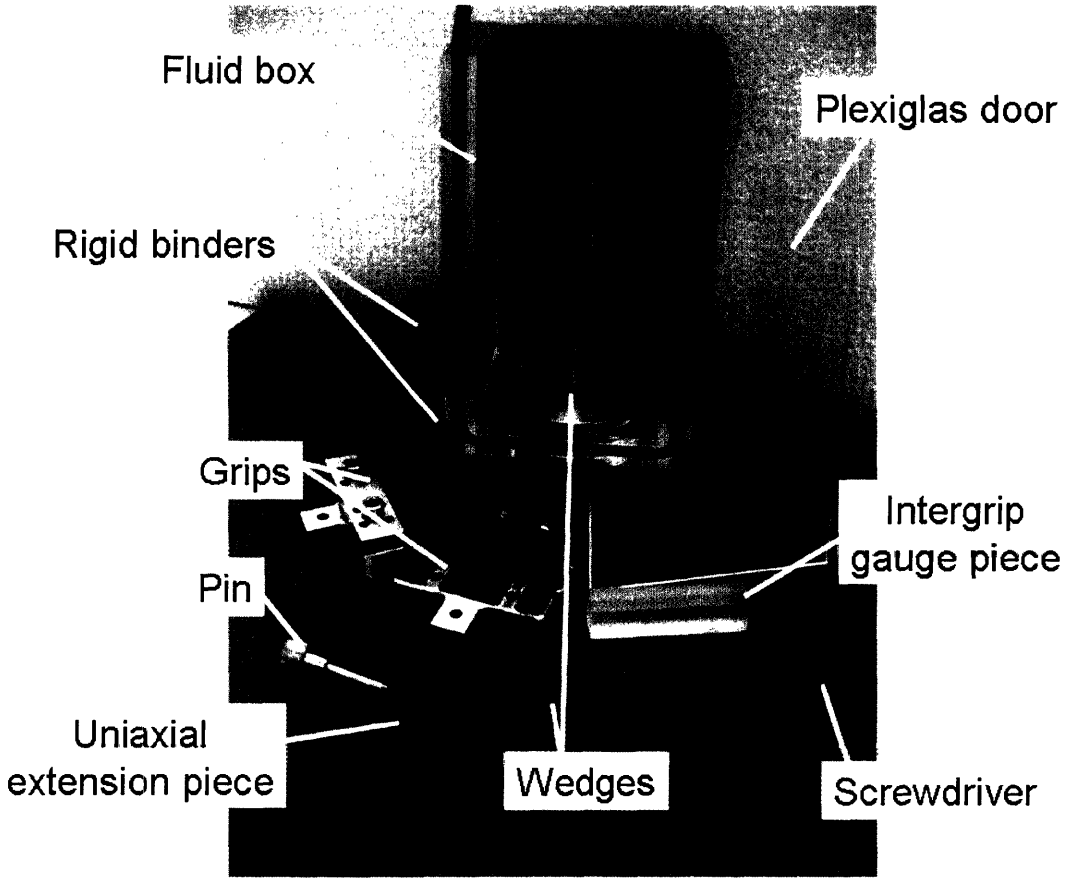

Figure B-3: Uniaxial testing fixtures and accessories.

- 12in.×18in. Self-healing cutting mat (Fiskars Catalog #86117097)
- Uniaxial testing features and accessories (Figure B-3)
- Digital micro caliper

B.3.2 Procedure

Amnion specimen preparation and cutting

1. Follow steps 1-3 of protocol B.2 ("CA membrane cutting and loading").
2. Carefully separate amnion from chorion, starting from one corner and moving along the diagonal (Figure B-4, Step 1)
3. Let amnion sample sit for 2-3hrs at 4°C.
4. Cut approximate 6×25 mm^2 strips, using marked grid on mat and rotary cutter. Proceed with care. Make sure specimen remains hydrated.
5. Transfer all strips into saline solution.

Amnion testing

1. Collect one strip, using tweezers and plastic film as supporting plate. Lay membrane over uniaxial grip apparatus (bottom grip + intergrip gauge piece + upper grip + wedges + uniaxial extension piece) carefully, making sure not to damage the tissue. The specimen must be centered (Figure B-4, Step 2).
2. Screw upper grip carefully (make sure grip does not move while screwing) and measure specimen width with caliper (Figure B-4, Step 3).
3. Position grip apparatus vertically into fluid box (Figure B-4, Step 4). Fix bottom grip with pin and wedges.

4. Transfer uniaxial tension device to testing machine very carefully, holding the whole unit vertically to prevent grips from moving or falling.

5. Hydrate sample with saline. Make sure it hangs vertically.

6. Screw bottom grip with care. Do not move it laterally while screwing (Figure B-4, Step 5).

7. Close fluid box with plexiglas door and rigid binders. Fill with saline (Figure B-4, Step 6).

8. Insert thermometer into fluid box and measure temperature.

9. Focus camera on specimen.

10. Make sure laptop is connected to camera and uniaxial test computer (controling Zwick machine). Check export measurement channels: make sure that Vic-Snap software picture file and Zwick Test file are properly correlated.

11. Start test and camera recording simultaneously.

12. Repeat steps 1-7 for each new test.

B.4 Thickness Measurement

B.4.1 Equipment and Materials

- 45 mm Rotary cutter (Fiskars Catalog #95217097)
- 45 mm Rotary straight blade (Fiskars Catalog #95287097)
- 12in.×18in. Self-healing cutting mat (Fiskars Catalog #86117097)
- Tweezers
- Timer

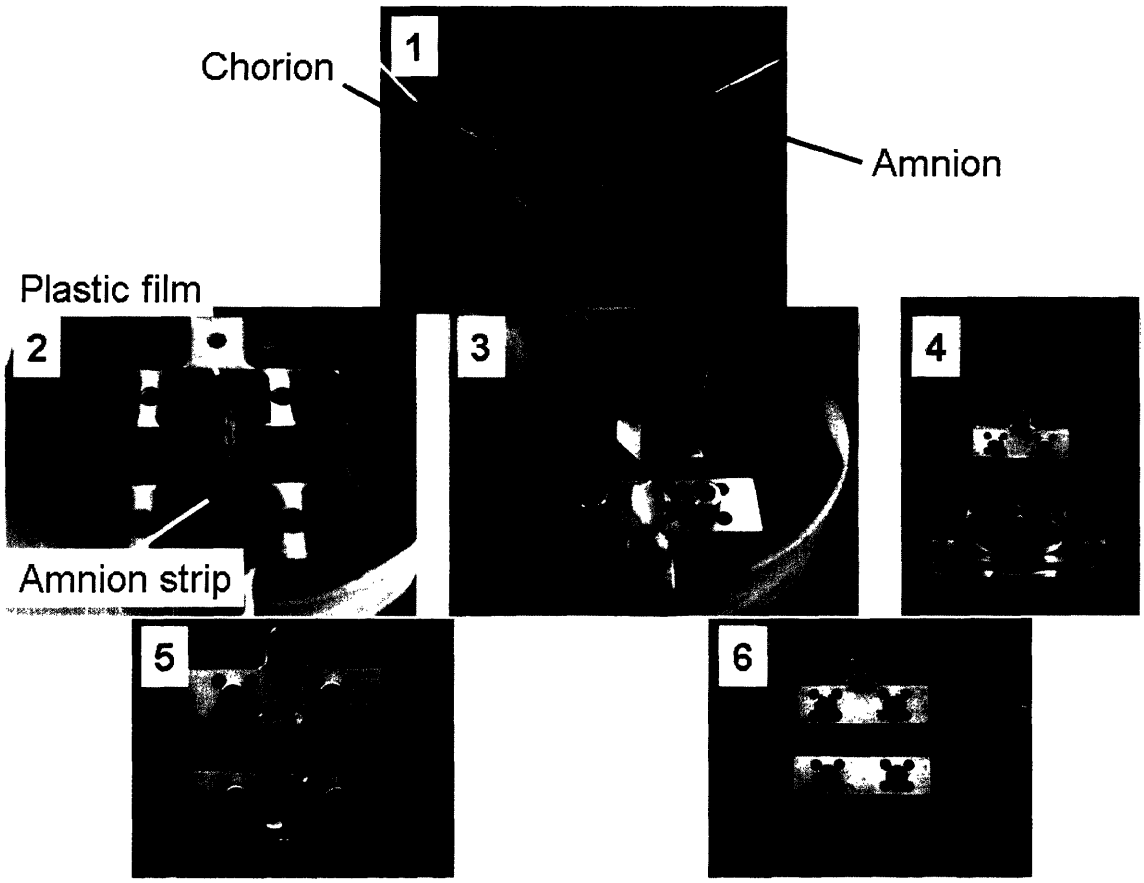

Figure B-4: Uniaxial testing: main steps.

- Petri dishes
- 24×50 mm^2 micro cover glasses (VWR Catalog #48393-081)
- Lab tissue (Delicate Task Wipers, Kimberley-Clark)
- Magnetic Induction Probe, V12 measurement stand with base (Fischer, probe ref. #ETA3)

B.4.2 Procedure

1. Follow steps 1-3 of protocol B.3 ("Amnion specimen preparation and cutting").
2. From both chorion and amnion, cut three ~1×3 cm^2 strips, using rotary cutter.
3. Lay each sample **flat** over lab tissue and allow it to dry for 4 minutes (2 minutes on each side). Make sure tissue is **completely unfolded.**
4. Position sample very carefully at center of cover glass, making sure it does not lie stretched. The edges of the cover glass must be kept dry. Place second glass on sample **without squeezing it.**
5. Place all 6 "sandwiched" samples in Petri dishes.
6. Place sample under magnetic induction probe. Perform one measurement at the center of the sample without reporting anything (so as to "flatten" the system). Then, carry out 6 independent measurements per sample on 6 evenly spaced spots over the microplate. Record thickness values.
7. Remove sample from cover glass, leaving possible water residues on it, and proceed as indicated in step 7 using the same two cover glasses with the water residues left in-between. Record thickness values of cover glass without tissue. Tissue thickness will be the difference between the two sets of measurements.

Appendix C

Biochemical assay protocols

C.1 Water content and Amnion/Chorion mass ratio measurement

C.1.1 Materials

- 20 mm punch (Boehm punch kit, Ref. #JLB330CM)
- Hammer
- Tweezers
- Aluminum foil
- Plastic cutting board
- Timer
- Lab tissue (Delicate Task Wipers, Kimberley-Clark)
- 1.5 mL Eppendorf tubes (VWR Catalog #20901-551)
- 600 mL Fast-Freeze flask (VWR Catalog #26675-308)

C.1.2 Procedure

1. Lay CA membrane flat over aluminum foil. **Make sure tissue is perfectly unfolded.**
2. Punch out CA specimens.
3. Let CA punched discs sit in saline.
4. Take out **one CA sample at a time.** Separate amnion from chorion and lay each layer flat over lab tissue for 4 minute drying (2 minutes on each side).
5. Place each sample into preweighed Eppendorf tubes.
6. Weigh tissue in preweighed tubes and record wet weight.
7. Freeze-dry samples for approximately 16 hours.
8. Record dry tissue weight.
9. The tissue water content in % is defined as: $\frac{m_{wet}^{tissue} - m_{dry}^{tissue}}{m_{wet}^{tissue}} \times 100$.
10. The amnion/chorion dry and wet mass ratios (%) are defined respectively as:

$$\frac{m_{dry}^{Amnion}}{m_{dry}^{Chorion}} \times 100 \text{ and } \frac{m_{wet}^{Amnion}}{m_{wet}^{Chorion}} \times 100.$$

C.2 Pulverization and Homogenization for Collagen and GAG Content Assays

C.2.1 Materials

- 20 mm and 12 mm punches (Boehm punch kit, Ref. #JLB330CM)
- Liquid nitrogen
- Thermo-flask
- Alumninum foil

- Plastic cutting board
- Tweezers
- Stainless steel biopulverizer (see [50])
- Hammer
- 1.5 mL Eppendorf tubes (VWR Catalog #20901-551)

C.2.2 Procedure

1. Separate amnion from chorion.
2. Cool biopulverizer for at least 10 minutes in liquid nitrogen
3. Lay each membrane flat over aluminum foil.
4. Punch out amnion and chorion samples (2×20 mm and 2×12 mm punched samples are needed per amnion and chorion sample respectively).
5. Wrap punched samples in aluminum foil and cool in liquid nitrogen for at least 2 minutes.
6. After 10 minutes of cooling, assemble biopulverizer on lab bench.
7. Remove tissue from liquid nitrogen and aluminum foil and place in the biopulverizer well.
8. Smash tissue inside biopulverizer well with hammer and pestle.
9. Gently tap out smashed tissue (it will resemble a flat pancake). Place about half of tissue pancake into Eppendorf tubes (tubes must be preweighed only for the GAG content assay).
10. Place tissue immediately into -80°C freezer for temporary storage.

C.3 Pulverization and Homogenization for Collagen Extractability Assay

C.3.1 Materials

- Timer
- Lab tissue (Delicate Task Wipers, Kimberley-Clark)
- 12 mL Kimax tubes with PTFE-faced Rubber Lined Cap (VWR Catalog #89001-480)
- All materials needed for Protocol C.2 (except for Eppendorf tubes)

C.3.2 Procedure

1. Remove CA membrane from saline.
2. Separate amnion from chorion.
3. Lay each membrane **flat** over lab tissue and allow it to dry for 4 minutes (2 minutes on each side). Make sure tissue is **completely unfolded.**
4. Follow steps 2-8 of previous protocol for tissue pulverization.
5. Gently tap out pulverized tissue and place about half of tissue pancake into **preweighed** Kimax tubes.
6. Weigh tissue in preweighed tube and record wet weight. Place tissue immediately into -80°C freezer for temporary storage.

C.4 Collagen Content - Tissue Preparation for the Hydroxyproline Assay

C.4.1 Materials

- 12 mL Kimax tubes with PTFE-faced Rubber Lined Cap (VWR Catalog #89001-480)

- 6N Hydrochloric Acid (HCl)

C.4.2 Procedure

1. Follow Protocol C.2 for tissue preparation.
2. Freeze dry frozen pulverized tissue for about 16 hours.
3. Weigh freeze dried tissue in Eppendorf tubes and carefully transfer tissue into Kimax tubes. Weigh Eppendorf tubes with tissue residues. Derive dry transferred tissue weight.
4. Add 1mL of 6N HCl to each sample and vortex.
5. Place samples in oven at ~115°C for hydrolyzation (20 hours).
6. After hydrolyzation, follow hydroxyproline assay [50,72]. Hydroxyproline content is measured per dry tissue weight. Collagen is measured in a 7.64:1 mass ratio to hydroxyproline.

C.5 Sulfated Glycosaminoglycan Content - DMMB assay

C.5.1 Materials

- Water bath
- Protease k (Sigma-Aldrich Catalog #C4384)
- DMMB dye (Dimethylmethylene blue dye, Polyscience INC)
- Molecular Devices micro-array spectrophotometer

C.5.2 Procedure

1. Follow Protocol C.2 for tissue preparation.
2. Freeze dry frozen tissue for about 16 hours.
3. Weigh dry tissue in preweighed Eppendorf tubes. Record dry tissue weight.
4. Add 1 mL of protease k solution (0.3 mg/mL) to each sample.
5. Place samples in 60°C water bath for 24 hours.
6. Place samples in 100°C water bath for 10 minutes to stop protease k digest.
7. For the DMMB assay, place 20 μL of digested tissue into microplate wells with 200 μL of DMMB dye.
8. Follow DMMB assay [50,73].

C.6 Collagen Extractability Assay

C.6.1 Materials

- Glacial Acetic Acid
- Pepsin (Sigma-Aldrich Catalog #P6887)
- Laboratory Rocker
- Centrifuge

C.6.2 Procedure

1. Follow Protocol C.3 for tissue preparation.
2. Make acetic acid extraction solution (150 μL/mg of wet tissue). Dilute Glacial Acetic Acid (17M) to 0.5M with deionized water. Dissolve 1mg/mL of pepsin into 0.5M acetic acid. Vortex solution and keep on ice.

3. Add acetic acid/pepsin extraction solution to frozen pulverized tissue (150 μL/mg of wet tissue) and vortex. Tissue pancake should break into small pieces.

4. Place samples on lab rocker in 4°C refridgerator for two and half days (ie 60 hours). Shake and flip over tubes every 12 hours.

5. Centrifuge samples at 15,000 g for one hour.

6. Separate supernatant and tissue pellet. Pipette supernatant into separate Kimax tubes. Store supernatant and tissue pellet at -80°C for at least half an hour.

7. Freeze dry frozen solid supernatant and tissue pellet for 24 hours.

8. Add 1 mL of 6N HCl to samples and vortex thoroughly.

9. Place samples in oven at ~115°C for hydrolyzation (20 hours).

10. After hydrolyzation, follow hydroxyproline assay [50,72].

11. The collagen extractability level for the tissue is defined in % as:

$\frac{C^{tissue}_{\text{supernatant}}}{C^{tissue}_{\text{supernatantt}}+C^{tissue}_{pellet}} \times 100$, where C refers to the collagen concentration in Kimax tube.

Appendix D

Pressurized Bulge Test Engineering Drawings

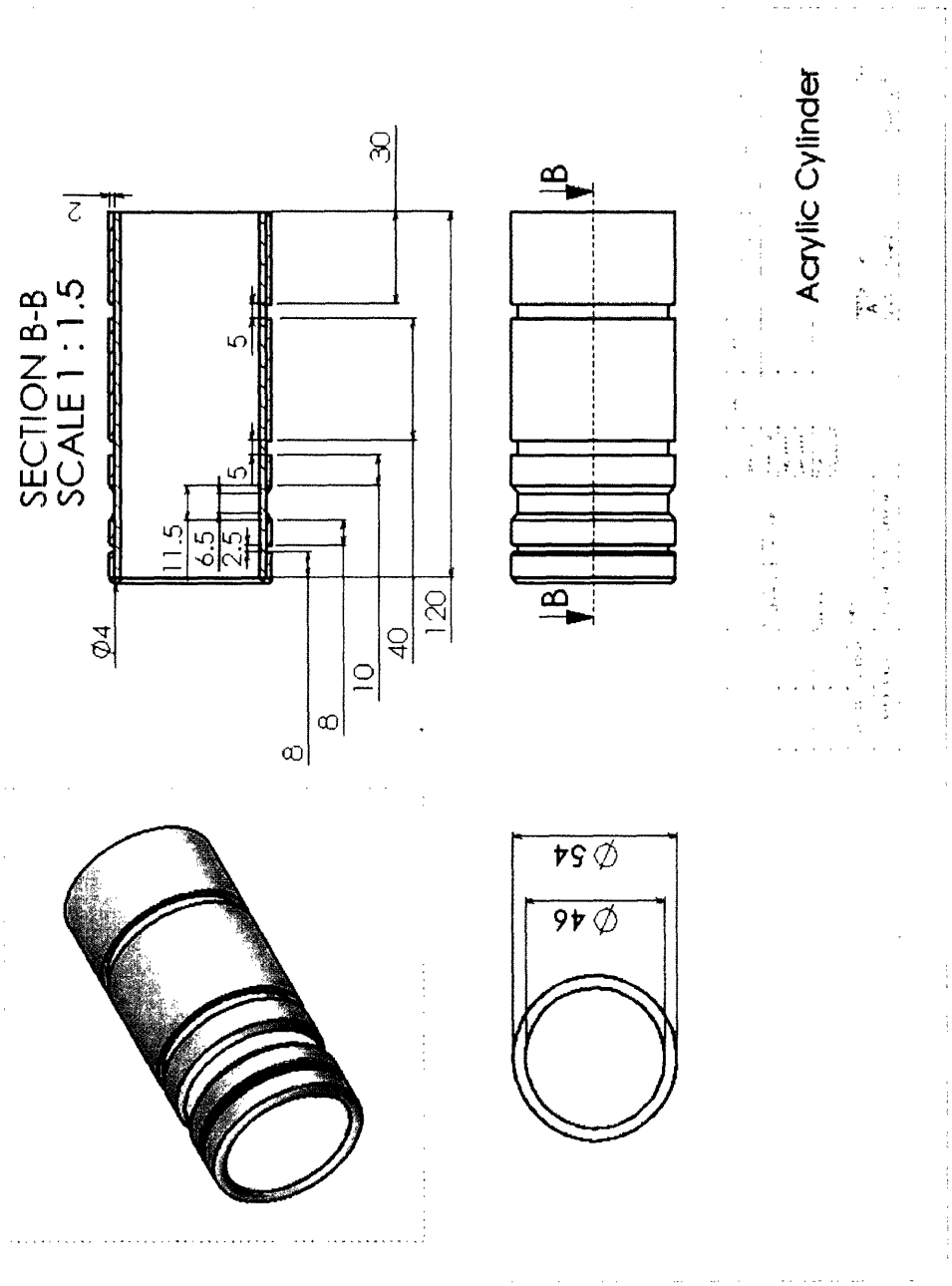

Figure D-1: Acrylic cylinder engineering drawing (dimensions are in mm).

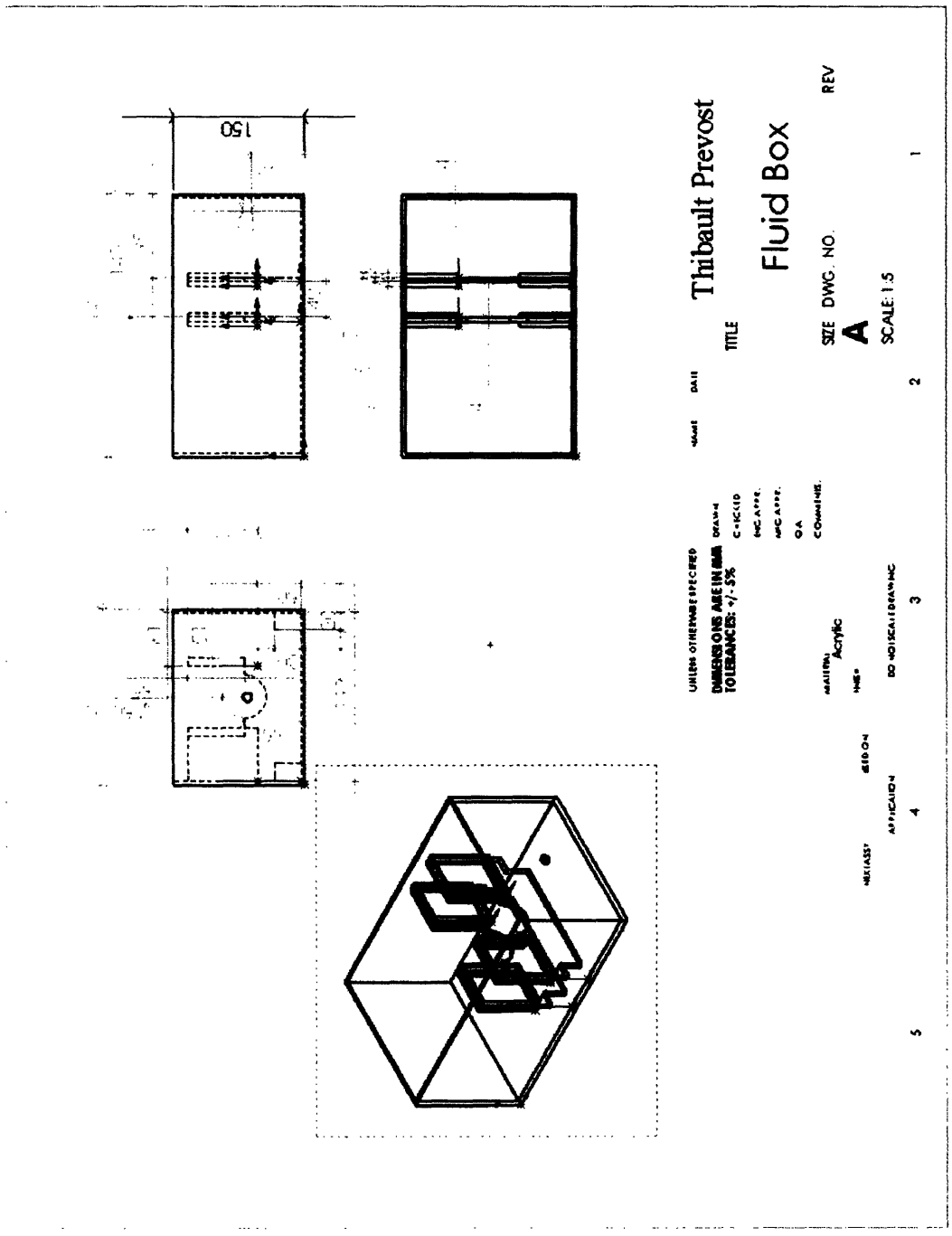

Figure D-2: Fluid box engineering drawing (dimensions are in mm).

Appendix E

Matlab m-files for Image Analysis

```
function imageseries = importimageseries(membrane,lastpixel,toppixel,bottompixel,leftedge,rightedge,
lastinstantframe,frequency,folder)
```

```
imageseries = [];
firstseries = [];
x = [];
files = dir(fullfile);
y = 1;

for x = firstinstantframe:
    if length(regexp(files(x).name, '.tif')) == 0
        temp = imread(strcat(folder, '\', files(x).name));
        level = graythresh(temp(:,:,1:lastpixel));
        temp = im2bw(temp(:,:,1:lastpixel), level);
        imageseries(:,:,y) = imfill(temp, 'holes');
        imageseries = imageseries(:,leftedge:rightedge,:);
        y = y+1;
        pack
    end
end

for x = firstinstantframe:frequency:length(files)
    if length(regexp(files(x).name, '.tif')) == 0
        temp = imread(strcat(folder, '\', files(x).name));
        level = graythresh(temp(:,:,1:lastpixel));
        temp = im2bw(temp(:,:,1:lastpixel), level);
        imageseries(:,:,y) = imfill(temp, 'holes');
        imageseries = imageseries(:,leftedge:rightedge,:);
        y = y+1;
        pack
    end
end

clear temp;
```

```
for x = 1:size(imageseries, 3)
    a = 1;
    topcontour=toppixel;
    bottomcontour=bottompixel-21;
    for y = 1:toppixel-1
        tracecoords(a,1,x) = 0;
        tracecoords(a,2,x) = y;
        a=a+1;
    end
    for y = toppixel:toppixel+20
        if length(find(imageseries(y,leftedge:rightedge,x) == 1, 1, 'last')) == 0
            tracecoords(a,1,x)=0;
            topcontour=topcontour+1;
        else
            tracecoords(a,1,x)=find(imageseries(y,leftedge:rightedge,x) == 1, 1, 'last')+leftedge-1;
        end
        tracecoords(a,2,x)=y;
        a=a+1;
    end
    for y = toppixel+21:bottompixel-21
        white_pixels=find(imageseries(y,:,x));
        tracecoords(a,1,x) = find_border(white_pixels);
        tracecoords(a,2,x) = y;
        a = a+1;
    end
    for y = bottompixel-20:bottompixel
        if length(find(imageseries(y,leftedge:rightedge,x) == 1, 1, 'last')) == 0
            tracecoords(a,1,x) = 0;
        else
            tracecoords(a,1,x)=find(imageseries(y,leftedge:rightedge,x) == 1, 1, 'last')+leftedge-1;
            bottomcontour=bottomcontour+1;
        end
        tracecoords(a,2,x)=y;
        a=a+1;
    end
    for y = bottompixel+1:size(imageseries,1)
        tracecoords(a,1,x)=0;
        tracecoords(a,2,x)=y;
        a=a+1;
    end
    topcontour;
    bottomcontour;
    x_contour=min(tracecoords(topcontour:bottomcontour,:,x));
    geometry(x,1)=topcontour;
    geometry(x,2)=bottomcontour;
    geometry(x,3)=bottomcontour-topcontour;
    geometry(x,4)=x_contour;
end
```

```
[illegible]
[illegible]
assignin([illegible], [illegible], [illegible]);
assignin([illegible], [illegible], [illegible]);
assignin([illegible], [illegible], [illegible]);
pack

[illegible]
function border_index = find_border(row)
if length(row)<=1
    border_index=0;
else
        a(1)=row(1)-1;
        for i=2:length(row)
            a(i)=row(i-1);
        end
            diff=row-a;
            [non_border_indices]=find(diff~=1);
            i=length(non_border_indices):-1:1
                if i==10
                    border_index=i;
                elseif (non_border_indices(i-10)~=non_border_indices(i-10)+1)
                    border_index=row(non_border_indices(i));
                    break
                end
            end
end
end

end
```

Bibliography

[1] *Premature Rupture of Membranes.* ACOG Practice Bulletin No. 1, June 1998. (Washington, D.C.: American College of Obstetricians and Gynecologists)

[2] Ventura SJ et al. *Report of Final Natality Statistics, 1995.* Monthly Vital Statistics Report; vol 45, no. 11, supp. Hyattsville, Maryland: National Center for Health Statistics, 1997.

[3] Parry S, Strauss JF. *Premature Rupture of the Fetal Membranes.* New England Journal of Medicine, 1998, 338: 663-670.

[4] Pritchard J. A. et al. *Williams Obstetrics*, 17th edition. Norwalk, Conn.: Appleton-Century-Crofts, 1985.

[5] Danforth DN et al. *The Microscopic Anatomy of the Fetal Membranes with Particular Reference to the Detailed Structure of the Amnion.* American Journal of Obstetrics and Gynecology, 1958, 75: 536-550.

[6] Bourne GL, Lacy D. *Ultra-Structure of Human Amnion and Its Possible Relation to the Circulation of Amniotic Fluid.* Nature, 1960, 186: 952-954.

[7] Bourne GL. *The Microscopic Anatomy of the Human Amnion and Chorion.* American Journal of Obstetrics and Gynecology, 1960, 79: 1070-1073.

[8] Bourne GL. *The Foetal Membranes, a Review of the Anatomy of Normal Amnion and Chorion and Some Aspects of Their Function.* Postgraduate Medical Journal, 1962, 38: 193-201.

[9] Oxlund H et al. *Biomechanical analysis of human chorioamniotic membranes.* European Journal of Obstetrics & Gynecology and Reproductive Biology, 1990, 34:247-55.

[10] Bryant-Greenwood GD. *The Extracellular Matrix of the Human Fetal Membranes: Structure and Function.* Placenta, 1998, 19: 1-11.

[11] Leppert PC, Woessner JF. *The Extracellular Matrix of the Uterus, Cervix and Fetal Membranes: Synthesis, Degradation and Hormonal Regulation.* Perinatology Press, Ithaca, New York, 1991.

[12] Alberts B et al. *Molecular Biology of the Cell*, 4th edition. Garland Science, New York, 2002.

[13] Brennan MJ et al. *Chondroitin/dermatan sulfate proteoglycan in human fetal membranes. Demonstration of antigenically similar proteoglycan in fibroblasts.* Journal of Biological Chemistry, 1984, 259:13742-50.

[14] Meinert M et al. *Proteoglycans and hyaluronan in human fetal membranes.* American Journal of Obstetrics and Gynecology, 2001, 184:679-85.

[15] Schmidt MB et al. *Effects of Proteoglycan Extraction on the Tensile Behavior of Articular Cartilage.* Journal of Orthopaedic Research, 1990, Vol 8 No 3:353-63.

[16] Danielson KG et al. *Targeted disruption of decorin leads to abnormal collagen fibril morphology and skin fragility.* Journal of Cell Biology, 1997, 136:729-43.

[17] Roughley PJ, Lee ER. *Cartilage Proteoglycans: Structure and Potential Functions.* Microscopy Research and Technique, 1994, 28:385-97.

[18] Uldbjerg N, Danielsen CC. *A Study of the Interaction in Vitro between Type I Collagen and a Small Dermatan Sulphate Proteoglycan.* Biochemical Journal, 1988, 251:643-48.

[19] Malak TM, Bell SC. *Differential expression of the integrin subunits in human fetal membranes.* Journal of Reproduction and Fertility, 1994, 102:269-76.

[20] Casey ML, MacDonald PC. *Biomolecular processes in the initiation of parturition: decidual activation.* Clinical Obstetrics and Gynecology, 1988, 31:533-52.

[21] Lockwood CJ et al. *Fetal Fibronectin in cervical and vaginal secretions as a predictor of preterm delivery.* New England Journal of Medicine, 1991, 325:669-74.

[22] Yamada KM. *Fibronectin and other cell interactive glycoproteins.* Cell Biology of Extracellular Matrix, pp. 111-139, Hay ED, 2nd edition, 1991. New York & London: Plenum Press.

[23] Ruoslahti E. *Integrins as receptors for extracellular matrix.* Cell Biology of Extracellular Matrix, pp. 343-359, Hay ED, 2nd edition, 1991. New York & London: Plenum Press.

[24] Champliaud MF et al. *Human amnion contains a novel laminin variant, laminin 7, which like laminin 6, covalently associates with laminin 5 to promote stable epithelial-stromal attachment.* Journal of Cell Biology, 1996, 132:1189-98.

[25] Malak TM, Bell SC. *Distribution of fibrillin-containing microfibrils and elastin in human fetal membranes: a novel molecular basis for membrane elasticity.* American Journal of Obstetrics and Gynecology, 1994, 171:195-205.

[26] Hannah ME et al. *Induction of labor compared with expectant management for prelabor rupture of the membranes at term.* New England Journal of Medicine, 1996, 334:1005-10.

[27] Mercer BM, Arheart KL. *Antimicrobial therapy in expectant management of preterm premature rupture of the membranes.* Lancet, 1995, 346:1271-79.

[28] Schucker JL, Mercer BM. *Midtrimester premature rupture of the membranes.* Seminars in Perinatology, 1996, 20:389-400.

[29] Gomez R et al. *Premature labor and intraamniotic infection.* Clinics in Perinatology, 1995, 22:281-342.

[30] Arias F et al. *Maternal placental vasculopathy and infection: two distinct subgroups among patients with preterm labor and preterm ruptured membranes.* American Journal of Obstetrics and Gynecology, 1993, 168:589-91.

[31] Toppozada MK et al. *Role of repeated stretching in the mechanism of timely rupture of the membranes.* American Journal of Obstetrics and Gynecology, 1970, 108:243-49.

[32] Arikat S et al. *Separation of amnion from choriodecidua is an integral event to the rupture of normal term fetal membranes and constitutes a significant component of the work required.* American Journal of Obstetrics and Gynecology, 2006, 194:211-17.

[33] French JI, McGregor JA. *The pathobiology of premature rupture of membranes.* Seminars in Perinatology, 1996, 20:344-68.

[34] Novak-Antolic Z et al. *Rupture of the membranes and postpartum infection.* European Journal of Obstetrics & Gynecology and Reproductive Biology, 1997, 71:141-46.

[35] Weiner CP et al. *Normal values for human umbilical venous and amniotic fluid pressures and their alteration by fetal disease.* American Journal of Obstetrics and Gynecology, 1989, 161:714–17.

[36] Skinner SJM et al. *Collagen Content of Human Amniotic Membranes: Effect of Gestation Length and Premature Rupture.* Obstetrics and Gynecology, 1981, 57:487-89.

[37] Kanayama N et al. *Collagen types in normal and prematurely ruptured amniotic membranes.* American Journal of Obstetrics and Gynecology, 1985, 153:899-903.

[38] Evaldson GR et al. *Is the Collagen Content Reduced when the Fetal Membranes Rupture?* Gynecologic and obstetric Investigation, 1987, 24:92-94.

[39] Halaburt JT et al. *The concentration of collagen and the collagenolytic activity in the amnion and the chorion.* European Journal of Obstetrics & Gynecology and Reproductive Biology, 1989, 31:75-82.

[40] Vadillo-Ortega F et al. *Collagen Metabolism in Premature Rupture of Amniotic Membranes.* Obstetrics and Gynecology, 1990, 75:84-88.

[41] Hampson V et al. *Amniotic membrane collagen content and type distribution in women with preterm premature rupture of the membranes in pregnancy.* British Journal of Obstetrics and Gynaecology, 1997, 104:1087-91.

[42] MacDermott RIJ, Landon CR. *The hydroxyproline content of amnion and prelabour rupture of the membranes.* European Journal of Obstetrics & Gynecology and Reproductive Biology, 2000, 92:217-21.

[43] Barabas AP. *Ehlers-Danlos syndrome: associated with prematurity and premature rupture of foetal membranes; possible increase in incidence.* BMJ, 1966, 5515:682-84.

[44] Offenbacher S et al. *Periodontal infection as a possible risk factor for preterm low birth weight.* Journal of Periodontology, 1996, 67:Suppl:1103-13.

[45] Bryant-Greenwood GD, Millar LK. *Human Fetal Membranes: Their Preterm Premature Rupture.* Biology of Reproduction, 2000, 63:1575-79.

[46] Sato T et al. *Hormonal regulation of collagenolysis in uterine cervical fibroblasts: modulation of synthesis of procollagenase, prostromelysin and tissue inhibitor of metalloproteinases (TIMP) by progesterone and oestradiol-17 beta.* Biochemical Journal, 1991, 275:645-50.

[47] Rajabi M et al. *Hormonal Regulation of interstitial collagenase in the uterine cervix of the pregnant guinea pig.* Endocrinology, 1991, 128:863-71.

[48] Qin X et al. *An autocrine/paracrine role of human decidual relaxin. II. Stromelysin-1 (MMP-3) and tissue inhibitor of matrix metalloproteinase-1 (TIMP-1).* Biology of Reproduction, 1997, 56:812-20.

[49] McGregor JA et al. *Bacterial Protease-Induced Reduction of Chorioamniotic Membrane Strength and Elasticity.* Obstetrics and Gynecology, 1987, 69:167-74.

[50] Myers KM. *Mechanical and Biochemical Properties of Human Cervical Tissue.* Master of Science Thesis, Massachusetts Institute of Technology, 2005.

[51] Skinner SJM, Liggins GC. *Glycosaminoglycans and collagen in human amnion from pregnancies with and without premature rupture of the membranes.* Journal of Developmental Physiology, 1981, 3:111-21.

[52] Helmig R et al. *Different biomechanical properties of human fetal membranes obtained before and after delivery.* European Journal of Obstetrics & Gynecology and Reproductive Biology, 1993, 48:183-89.

[53] Oyen ML et al. *Uniaxial stress-relaxation and stress-strain responses of human amnion.* Journal of Materials Science: Materials in Medicine, 2004, 15:619-24.

[54] Schober EA et al. *Resistance of Fetal Membranes to Concentrated Force Applications and Reconciliation of Puncture and Burst Testing.* Annals of Biomedical Engineering, 1994, 22:540-48.

[55] Oyen ML et al. *Mechanical failure of human fetal membrane tissues.* Journal of Materials Science: Materials in Medicine, 2004, 15:651-58.

[56] Polishuk WZ et al. *The Physical Properties of Fetal Membranes.* Obstetrics and Gynecology, 1962, 20:204-10.

[57] Al-Zaid NS et al. *Bursting pressure and collagen content of fetal membranes and their relation to premature rupture of the membranes.* British Journal of Obstetrics and Gynaecology, 1980, 87:227-29.

[58] Lavery JP et al. *The Viscoelastic Nature of Chorioamniotic Membranes.* Obstetrics and Gynecology, 1977, 50:467-72.

[59] Lavery JP, Miller CE. *Deformation and creep in the human chorioamniotic sac.* American Journal of Obstetrics and Gynecology, 1979, 134:366-75.

[60] Miller CE et al. *Determination of Elastic Parameters For Human Fetal Membranes.* Journal of Rheology, 1979, 23:57-78.

[61] Lavery JP et al. *The Effect of Labor on the Rheologic Response of Chorioamniotic Membranes.* Obstetrics and Gynecology, 1982, 60:87-92.

[62] Yannas IV, Comninou M. *Dependence of Stress-Strain Nonlinearity of Connective Tissues on the Geometry of Collagen Fibers.* Journal of Biomechanics, 1976, 9:427-33.

[63] Oyen ML et al. *Uniaxial and biaxial mechanical behavior of human amnion.* Journal of Materials Research, 2005, 20:2902-09.

[64] Parry-Jones E, Priya S. *A study of the elasticity and tension of fetal membranes and of the relation of the area of the gestational sac to the area of the uterine cavity.* British Journal of Obstetrics and Gynaecology, 1976, 83:205-12.

[65] Millar LK et al. *Fetal membrane distention: Determination of the intrauterine surface area and distention of the fetal membranes preterm and at term.* American Journal of Obstetrics and Gynecology, 2000, 182:128-34.

[66] Evans EA, Skalak R. *Mechanics and Thermodynamics of Biomembranes.* CRC Press, Inc., Boca Raton, Florida, USA, 1980.

[67] Fung YC. *Biomechanics: Mechanical Properties of Living Tissues,* 2nd edition. Springer-Verlag, New York, USA, 1993.

[68] Hansen JC et al. *Influence of network topology on the elasticity of the red blood cell membrane skeleton.* Biophysical Journal, 1997, 72:2369-81.

[69] Discher DE et al. *Simulations of the Erythrocyte Cytoskeleton at Large Deformation. II. Micropipette Aspiration.* Biophysical Journal, 1998, 75:1584-97.

[70] Li J et al. *Spectrin-Level Modeling of the Cytoskeleton and Optical Tweezers Stretching of the Erythrocyte.* Biophysical Journal, 2005, 88:3707-19.

[71] Dao M et al. *Molecularly based analysis of deformation of spectrin network and human erythrocyte.* Biophysical Journal, in press.

[72] Stegeman H, Stalder K. *Determination of hydroxyproline.* Clinica Chemica Acta, 1967, 18:267-73.

[73] Farndale RW et al. *A direct spectrophotometric microassay for sulfated glycosaminoglycans in cartilage cultures.* Connective Tissue Research, 1982, 9:247-48.

[74] Febvay S. *A three-dimensional constitutive model for the mechanical behavior of cervical tissue.* Master of Science Thesis, Massachusetts Institute of Technology, 2003.

[75] Qi HJ et al. *A Constitutive Model for the Stress-Strain Behavior of Biomacromolecular Networks Containing Folded Domains.* Submitted to Biophysical Journal, 2005.

[76] Treloar LRG. *The Physics of Rubber Elasticity.* Oxford University Press, 1975.

[77] Kuhn W, Grühn F. *Beziehungen zwischen elastischen Konstanten und Dehnungsdoppelbrechung hochelastischer Stoffe.* Kolloid-Z, 1942, 101:248-71.

[78] Boyce MC et al. *Constitutive Model for the Finite Deformation Stress-Strain Behavior of Poly(Ethylene Terephtalate) Above the Glass Transition.* Polymer, 2000, 41:2183-2201.